

AdS₃ spacetime wormhole fluctuations and their impact on false vacuum decay

Hong Wang^a and Jin Wang^{b,1}

^a*State Key Laboratory of Electroanalytical Chemistry, Changchun Institute of Applied Chemistry, Chinese Academy of Sciences, Changchun 130022, China*

^b*Department of Chemistry and Department of Physics and Astronomy, State University of New York at Stony Brook, NY 11794, USA*

Abstract

In this work, we studied the boundary wormhole fluctuations of AdS₃ spacetime and their impact on false vacuum decay. The model consists of three dimensional general relativity coupled to a real scalar field with self-interaction potential. Our analysis focuses on handlebody spacetimes, which correspond to boundary wormhole fluctuations. These fluctuations result in variations in the spacetime genus. Using the dilute wormhole gas approximation, we computed the boundary wormhole creation rate in the semiclassical region. Our results indicate that boundary wormholes are more likely to be created in spacetimes with larger absolute values of the cosmological constant. Furthermore, we find that smaller wormholes are more easily created compared to larger ones. Additionally, we investigated the impact of boundary wormhole fluctuations on false vacuum decay. The vacuum decay rate increases when the effects of wormhole fluctuations are considered. We show that all results remain qualitatively unchanged when certain parameter values are varied.

¹Corresponding author, jin.wang.1@stonybrook.edu

Contents

1	Introduction	2
2	Boundary wormhole fluctuations and false vacuum decay	4
3	The tunneling action	9
3.1	The total tunneling action	9
3.2	Representing the tunneling action in the Siegel upper half space	19
4	Integration for the non-equivalent boundary wormhole fluctuations	22
5	The tunneling rate	30
5.1	Boundary wormhole creation rate	30
5.2	Boundary wormhole fluctuations influence on the false vacuum decay .	37
6	Conclusions and discussions	40
A	Schottky parametrization of the AdS_3 handlebody	42
B	Relationship between the period matrix and the Schottky group	46
C	Derivation for the vacuum decay seed B_{seed}	49
D	Derivation for equation (46)	50

1 Introduction

The local properties of classical spacetime are determined by the metric, which can be obtained by solving the Einstein equations. In addition to local properties, spacetime may possess non-trivial topological invariants, such as genus and homology groups [1]. These topological invariants are global properties of spacetime and are independent of the metric [2, 3]. This independence implies that the Einstein equations do not determine the topological invariants. Moreover, the topological invariants of spacetime may correspond to observable effects [1, 4, 5]. It is widely believed that quantum fluctuations can change the topological invariants of spacetime [2, 6, 7]. Thus, topological invariants are important topics in both classical and quantum gravity.

The renormalization problem of four dimensional quantum gravity remains unresolved [8]. However, three dimensional quantum gravity is renormalizable and lacks bulk graviton excitations [9]. It has been shown that three dimensional Einstein pure gravity (with no matter except dark energy) is equivalent to the Chern-Simons topological field theory [9]. Thus, three dimensions provide an ideal framework for studying topological issues in quantum gravity. Despite our universe being at least macroscopically four dimensional, insights from three dimensional studies are believed to offer valuable perspectives [7, 9].

When the cosmological constant is positive or zero, there is a finite class of topologically non-equivalent three dimensional spacetimes. In contrast, with a negative cosmological constant, there is an infinite class of topologically non-equivalent three dimensional spacetimes [10]. Thus, AdS_3 spacetime exhibits rich topological properties. The conformal boundary of the genus zero Euclidean AdS_3 spacetime is a cylinder. All genus one AdS_3 spacetimes are handlebodies, whereas higher genus AdS_3 spacetimes can be either handlebodies or non-handlebodies [11–13]. A handlebody has only one boundary, while a non-handlebody has multiple disconnected boundaries [11–14]. That is, in a non-handlebody spacetime, the boundaries are connected only through the bulk and cannot be connected through the boundary itself [14]. Studies by Maldacena, Maoz, and other researchers have highlighted certain puzzles associated with the non-handlebody solutions of the Einstein equations in the context of AdS/CFT duality [14–18]. However, in three dimensional spacetime, some research suggests that the

contribution of non-handlebody spacetimes to the partition function is small compared to that of handlebody spacetimes [12, 13]. Therefore, for simplicity, this work focuses on AdS_3 handlebody spacetimes.

Significant theoretical progress has been achieved in studying spacetimes with non-zero genus. In 1989, Witten demonstrated that, when the cosmological constant is zero, the partition function of three-dimensional pure quantum gravity can be expressed as the integral of the Ray-Singer analytic torsion (a topological invariant) over the moduli space of the Einstein equations [2]. In 1993, Carlip introduced a method to compute the partition function of three dimensional quantum gravity, accounting for worm-hole fluctuations in the limit of a small cosmological constant. He showed that the partition function exhibits divergence [19]. In 2000, Krasnov showed that the regularized Einstein-Hilbert action of the AdS_3 handlebody spacetime is equivalent to the Takhtajan-Zograf action, which corresponds to the action of the Liouville field defined on the two dimensional boundary of the bulk AdS_3 spacetime [20]. Subsequently, Takhtajan, Teo, and Park proved that this equivalence holds even when the boundary surface contains elliptic or parabolic singularities (cone points or punctures, respectively) [21–23]. These findings strongly support the $\text{AdS}_3/\text{CFT}_2$ duality. In recent years, researchers have employed new methods to study the partition function of thermal AdS_3 spacetime, incorporating contributions from boundary graviton excitations [24, 25]. Other significant studies have also been undertaken; see [26–38] and references therein. We will not enumerate them all here.

Despite significant progress in three dimensional topological quantum gravity, the challenge of wormhole fluctuations remains unresolved [2, 19]. In this work, we aim to study the boundary wormhole fluctuations of AdS_3 spacetime and their influence on false vacuum decay. All spacetimes considered are AdS_3 handlebody solutions of the Euclidean Einstein equations, which correspond to the boundary wormhole fluctuations. The local properties of various AdS_3 handlebodies are identical, as they are determined by the Euclidean Einstein equations, while their global structures differ [20]. The model consists of a real scalar field minimally coupled to three dimensional general relativity. The scalar potential has two minimal values, and the difference between these values is assumed to be small, ensuring the validity of the thin wall approximation. When the

scalar field occupies one of the potential minima, it acts as a cosmological constant. This model describes both wormhole fluctuations and false vacuum decay, with no restriction on the cosmological constant being close to zero.

The Euclidean AdS_3 spacetime action is divergent and requires regularization [20]. The process of boundary wormhole fluctuation is accompanied by changes in the spacetime genus. We work in the semiclassical region and use the Euclidean path integral approach to compute the boundary wormhole creation rate. Using the dilute wormhole gas approximation, we transform the tunneling action from the Schottky space to the Siegel upper half space. This approximation simplifies the integral domain, which is a subspace of the fundamental domain of the modular group $\text{Sp}(2g, \mathbb{Z})$ in the Siegel upper half space. Consequently, integration over the physically non-equivalent AdS_3 spacetimes becomes feasible.

Our results indicate that boundary wormholes are more easily created in AdS_3 spacetime with a more negative cosmological constant. We find that small boundary wormhole are more likely to occur than larger ones. This suggests that large scale wormholes are difficult to create. We also studied the influence of boundary wormhole fluctuations on AdS_3 vacuum decay. Both the dilute instanton gas approximation and the dilute wormhole gas approximation were used. Our analysis shows that including boundary wormhole fluctuations increases the vacuum decay rate. We also observe that defining the initial state within our framework breaks modular symmetry. Although there are two unspecified parameters in our model, we demonstrate that their values do not qualitatively affect the results. Throughout this study, we work in units where $8\pi G = \hbar = k_B = c = 1$.

2 Boundary wormhole fluctuations and false vacuum decay

A simple model for studying quantum gravity consists of three dimensional general relativity coupled to a real scalar field with a self-interaction potential. The Euclidean action for this model is given by [39]

$$S_E = \int dx^3 \sqrt{g} \left\{ -\frac{1}{2}R + \frac{1}{2}g^{\mu\nu} \partial_\mu \phi \partial_\nu \phi + V(\phi) \right\} + S_{GHY}. \quad (1)$$

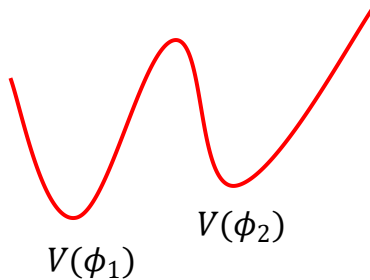


Figure 1: Diagram of the scalar potential. It has two minimal values, denoted as $V(\phi_1)$ and $V(\phi_2)$.

Here, S_E represents the Euclidean action of the total system. R and S_{GHY} represent the Ricci scalar and the Gibbons-Hawking-York surface term, respectively. ϕ represents the scalar field, and $V(\phi)$ represents the scalar potential. In this work, we focus on the case where the scalar potential has two minimal values, as shown in figure 1. These minimal values are labeled as $V(\phi_1)$ and $V(\phi_2)$, with $V(\phi_1) < V(\phi_2) < 0$. Usually, the states $V(\phi_1)$ and $V(\phi_2)$ are called the true vacuum state and the false vacuum state, respectively [40]. For simplicity, we assume $\epsilon = V(\phi_2) - V(\phi_1)$ to be a small quantity. In this case, the thin wall approximation is valid [40, 41]. Extending this model to scenarios where the potential has more local minimal values is straightforward.

The action (1) is generally valid regardless of the spacetime genus. The model defined by this action can describe both wormhole fluctuations and false vacuum decay. When the scalar field resides at one of the potential minima, it effectively serves as a cosmological constant, allowing the model to describe wormhole fluctuations. In another situation, if quantum fluctuations of the spacetime topological structure are neglected, the model (1) can be used to study false vacuum decay. In this work, we consider both wormhole fluctuations and false vacuum decay. Thus, it is necessary to include a scalar field in the model. The false (true) vacuum state $V(\phi_2)$ ($V(\phi_1)$) of the scalar field is equivalent to a cosmological constant. Thus, we may refer to $V(\phi_1)$ or $V(\phi_2)$ as a cosmological constant to emphasize its relationship with wormhole fluctuations. At other times, we refer to $V(\phi_1)$ and $V(\phi_2)$ as the true vacuum state and false vacuum state, respectively, to highlight the vacuum decay dynamics. Additionally, in some equations, we may use the symbol Λ to represent the cosmological constant for convenience. This flexibility in terminology are necessary to clearly describe different physical processes and to avoid confusion.

When the scalar field is in the state $V(\phi_1)$ or $V(\phi_2)$, the Einstein equations reduce to

$$R = 6\Lambda. \quad (2)$$

In our model, the value of the cosmological constant Λ equals $V(\phi_1)$ ($V(\phi_2)$) when the scalar field is in the state $V(\phi_1)$ ($V(\phi_2)$). Equation (2) admits infinitely many solutions [7, 11, 20, 42], all of which are AdS_3 spacetimes. These solutions can be categorized into handlebodies and non-handlebodies [11–13]. Some studies indicate that the quantum effects of handlebodies are dominant [12, 13]. Thus, for simplicity, we focus on AdS_3 handlebody solutions.

Although all solutions to equation (2) have the same local properties, their global properties differ [7, 20, 42]. In other words, different AdS_3 spacetimes may possess distinct topological invariants [7, 20, 42], which are not determined by equation (2). Locally, every point in any AdS_3 handlebody has the same Ricci scalar. Globally, however, various AdS_3 spacetimes may have different genus [7, 20, 42]. Figure 2 illustrates some of these solutions. The cylinder shown in figure 2(a) represents a genus zero AdS_3 spacetime. We will refer to it as the parent universe. Figures 2(a), 2(b) and 2(c) depict AdS_3 handlebodies of genus zero, one and three, respectively. The red strips in figure 2 represent boundary wormholes, which can be produced through quantum tunneling [6]. We refer to these processes as boundary wormhole fluctuations (BWFs). The handlebodies shown in figures 2(b) and 2(c) can be interpreted as processes through which boundary wormholes are created in the parent universe. Figure 2 clearly shows that BWFs alter the spacetime genus.

Locally, any AdS_3 handlebody is homogenous and isotropic. Thus, one can use the metric [39]

$$ds^2 = d\tau_E^2 + \rho(\tau_E)^2(d\theta^2 + \sin^2\theta d\varphi^2). \quad (3)$$

to describe the local properties of various AdS_3 handlebodies. Here, τ_E and $\rho(\tau_E)$ represent the Euclidean proper time and the scale factor, respectively. The parameters φ and θ range as $0 \leq \varphi \leq 2\pi$ and $0 \leq \theta \leq \pi$, respectively. Given any point P in an AdS_3 handlebody, there exists a neighborhood of P that is spherically symmetric. Within this neighborhood, the metric (3) is well defined. In the special case of a genus zero AdS_3 spacetime (the parent universe), the spacetime is globally homogeneous and

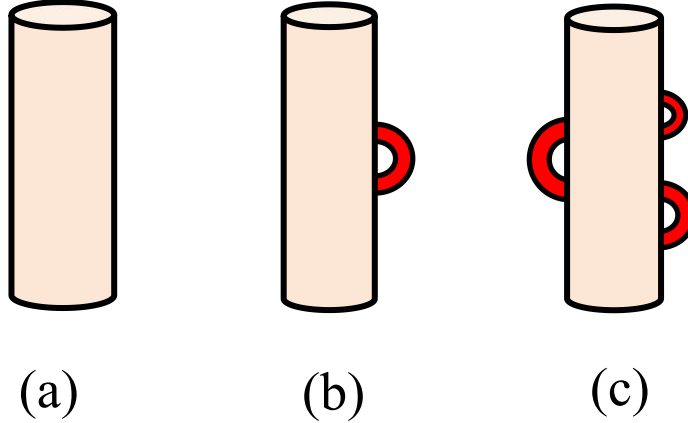


Figure 2: Diagram of various AdS_3 handlebodies. Figures (a), (b) and (c) represent the AdS_3 handlebody with genus zero, one and three, respectively. The cylinder represents the parent universe. The red strips represent the boundary wormholes.

isotropic, not just locally. Hence, the metric (3) is valid throughout the entire parent universe, and all properties of the parent universe can be described by it. However, higher genus AdS_3 handlebodies lack global spherical symmetry. Therefore, this metric cannot be globally applied to higher genus AdS_3 handlebodies.

Now consider false vacuum decay in the parent universe. In the semiclassical region, the Coleman-De Luccia theory gives the vacuum decay rate as [40]

$$\Gamma \approx \exp\left\{-\left(S_E(\phi_{\text{bounce}}) - S_E(\phi_2)\right)\right\} \equiv e^{-B}. \quad (4)$$

Here, ϕ_{bounce} represents the bounce solution of the scalar field. We refer to $S_E(\phi_2)$ as the background term, and B as the total tunneling action. In deriving equation (4), Both the thin wall approximation and the dilute instanton gas approximation are used. The bounce solution can be visualized as a three dimensional spherically symmetric bubble (the bounce bubble) embedded in a sea of false vacuum [40]. The radius of the bounce bubble $\bar{\rho}$ is determined by the condition $\partial B / \partial \bar{\rho} = 0$ [40]. Thus, the tunneling action can be written as $B = B_{\text{in}} + B_{\text{wall}} + B_{\text{out}}$, where B_{in} and B_{out} denote the tunneling actions inside and outside the bubble, respectively, and B_{wall} represents the tunneling action on the domain wall.

The background term and the bounce solution can be represented by figures 3(a) and 3(b), respectively. The blue ball in figure 3(b) represents the bubble. Inside

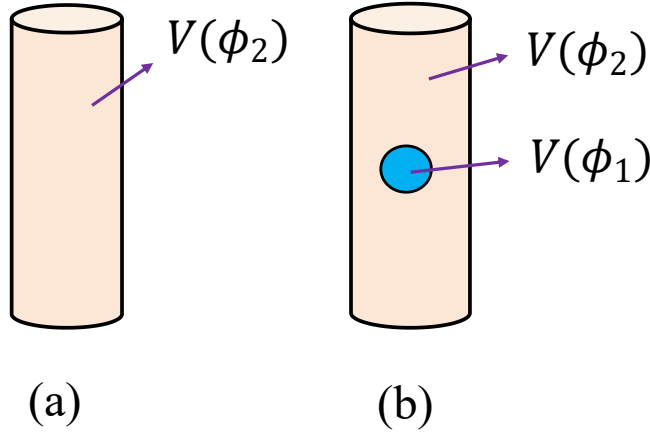


Figure 3: Diagram of false vacuum decay. Figures (a) and (b) represent the background term and the bounce solution, respectively. The blue ball in figure (b) represents the bubble.

and outside the blue ball, the cosmological constant takes the values $V(\phi_1)$ and $V(\phi_2)$, respectively. In figure 3(a), the scalar field is entirely in the state $V(\phi_2)$. Figure 3(b) describes the process of false vacuum decay. Comparing figures 3(a) and 3(b), one can see that false vacuum decay can also be interpreted as the creation of a bubble. Consequently, the vacuum decay rate can be understood as the bubble creation rate.

The dynamical equation of the scalar field in various AdS_3 spacetimes is the same. It is the Klein-Gordon equation. This implies that false vacuum decay can occur not only in the genus zero AdS_3 spacetime but also in higher genus AdS_3 spacetimes. In other words, bubble creation is possible in both genus zero and higher genus AdS_3 spacetimes, as illustrated in figure 4. To calculate the bubble creation rate (i.e., false vacuum decay rate), all possible modes of bubble creation must be considered. It is important to note that different modes of bubble creation correspond to different AdS_3 handlebodies, and these handlebodies can be interpreted as representing different BWFs. Therefore, summing over all possible modes of bubble creation is equivalent to summing over all BWFs. As a result, the total bubble creation rate (or total false vacuum decay rate) can be expressed as:

$$\Gamma_{tot} = \sum_{\mathcal{M}} e^{-B}. \quad (5)$$

Here, $\sum_{\mathcal{M}}$ represents the summation over all physically non-equivalent BWFs.

In the next section, we will demonstrate that the total tunneling action B varies

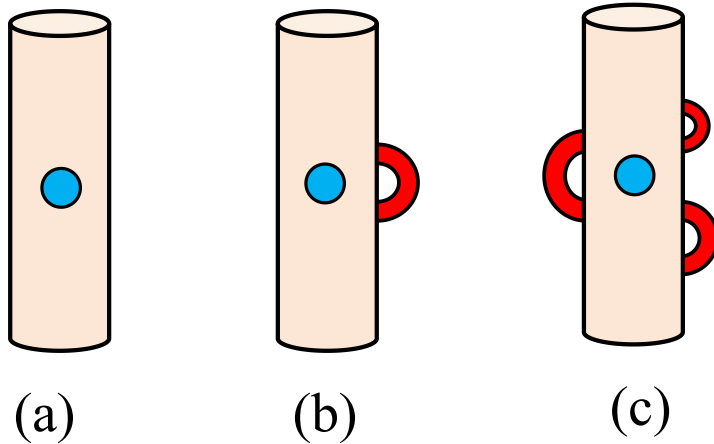


Figure 4: Diagram of false vacuum decay in various AdS_3 spacetimes. The cylinders represent the parent universe, while the blue balls and red strips represent the bubble and boundary wormholes, respectively.

depending on the specific mode of false vacuum decay. Obviously, if the effects of BWFs are neglected, equation (5) reduces to equation (4). Additionally, in section 5, we will show that once the total tunneling action B and the total tunneling rate Γ_{tot} for false vacuum decay are determined, various interesting properties of AdS_3 BWFs can be derived from these quantities. Therefore, deriving the total tunneling action B and the total tunneling rate Γ_{tot} are the main tasks of this study.

3 The tunneling action

3.1 The total tunneling action

In this section, we focus on calculating the total tunneling action B in high genus spacetimes. Although high genus spacetimes do not possess global spherical symmetry, one can always find a locally spherically symmetric region, as illustrated in figure 5. The bounce bubble (with radius denoted as $\bar{\rho}$) resides within the parent universe. Thus, a spherically symmetric region containing the bounce bubble can always be found, such as the region inside the green circle (representing a spherical surface with radius larger than $\bar{\rho}$) in figure 5. We denote the radius of this region as ρ_s ($\rho_s > \bar{\rho}$). The exact value of ρ_s is not important.

The region with radius smaller than ρ_s in figure 5 is chosen to have spherical sym-

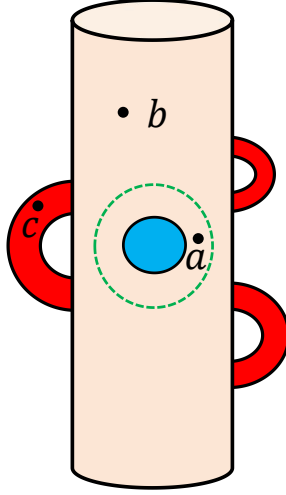


Figure 5: Diagram of false vacuum decay in a high genus AdS_3 handlebody. The cylinder represents the parent universe. The blue ball and the red strips represent the bubble and the boundary wormholes, respectively. The green circle represents a spherical surface that is larger than the brane of the bounce bubble.

metry. Thus, within this region, the metric (3) is well defined. Consequently, the Ricci scalar can be expressed as [39]

$$R = -4\frac{\ddot{\rho}}{\rho} + \frac{2}{\rho^2}(1 - \dot{\rho}^2), \quad (6)$$

where, $\dot{\rho} \equiv d\rho/d\tau_E$. Substituting equations (3) and (6) into equation (1), the Euclidean action (1) in the region $\rho \leq \rho_s$ can be written as

$$S_E(\rho \leq \rho_s) = \int d\theta d\varphi \int_0^{\rho_s} d\tau_E \sqrt{g} \left\{ -\frac{\dot{\rho}^2}{\rho^2} - \frac{1}{\rho^2} + \frac{1}{2}\dot{\phi}^2 + V(\phi) \right\}. \quad (7)$$

Here, $S_E(\rho \leq \rho_s)$ represents the Euclidean action for the region $\rho \leq \rho_s$ of the model defined by equation (1).

From equations (1) to (7), we utilize the fact that the Gibbons-Hawking-York surface term S_{GHY} is canceled out by the boundary term generated in the partial integral with respect to the Ricci scalar R . The Euclidean action plays a central role in the Euclidean path integral. In the semiclassical region, this method is widely used to study quantum gravity with a negative cosmological constant [6, 11, 19, 24, 25, 43]. Thus, we will use this method to study the model defined by equation (1).

From equation (7), the total Hamiltonian density (\mathcal{H}_{tot}) of the system in the region

$\rho \leq \rho_s$ is given by

$$\mathcal{H}_{tot} = \sqrt{g} \left\{ -\frac{\dot{\rho}^2}{\rho^2} + \frac{1}{\rho^2} + \frac{1}{2}\dot{\phi}^2 - V(\phi) \right\}. \quad (8)$$

General covariance requires the total Hamiltonian density to be zero [41, 44–46]. Using $\delta S_E / \delta \phi = 0$ and $\mathcal{H}_{tot} = 0$, one can obtain the dynamical equations [39]

$$\ddot{\phi} = \frac{\partial V}{\partial \phi}, \quad (9)$$

$$\dot{\rho}^2 = 1 + \rho^2 \left(\frac{1}{2}\dot{\phi}^2 - V(\phi) \right). \quad (10)$$

Equation (9) is the Klein-Gordon equation, while equation (10) is the Friedmann equation. Note that in equation (9), the Hubble drag term $2\dot{\rho}\dot{\phi}/\rho$ has been neglected, as it is small under the thin wall approximation [40].

Substituting equation (10) into equation (7), the Euclidean action (7) simplifies to

$$\begin{aligned} S_E(\rho \leq \rho_s) &= 2 \int d\theta d\varphi \int_0^{\rho_s} d\tau_E \sqrt{g} \left\{ \frac{-1}{\rho^2} + V(\phi) \right\} \\ &= \int d\theta d\varphi \int_0^{\rho_s} d\tau_E \sqrt{g} \mathcal{L}_{eff}(\phi). \end{aligned} \quad (11)$$

Here,

$$\mathcal{L}_{eff}(\phi) \equiv 2 \left\{ \frac{-1}{\rho^2} + V(\phi) \right\} \quad (12)$$

is defined as the effective Lagrangian density. Since the action $S_E(\rho \leq \rho_s)$ in equation (7) is valid in the spherically symmetric region $\rho \leq \rho_s$, the dynamical equations (9), (10) and the Euclidean action (11) are also valid in this region. More generally, regardless of the genus of the spacetime, if a given region is spherically symmetric, equations (9), (10) and (11) hold in that region. In equation (11), the Euclidean action does not depend on the terms $\dot{\rho}$ and $\dot{\phi}$. Thus, equation (11) is particularly convenient for calculating the total tunneling action B .

Denoting the effective Lagrangian density of the system in the region $\rho > \rho_s$ as $\mathcal{J}_{eff}(\phi)$. We assume that the coordinates (x'_1, x'_2, x'_3) are well defined in this region. Then, the Euclidean action of the system for the region $\rho > \rho_s$ can be formally expressed as

$$S_E(\rho > \rho_s) = \int_{\rho > \rho_s} dx'_1 dx'_2 dx'_3 \sqrt{g'} \mathcal{J}_{eff}(\phi). \quad (13)$$

Here, we use $S_E(\rho > \rho_s)$ to denote the Euclidean action for the region $\rho > \rho_s$. The symbol $\int_{\rho > \rho_s}$ represents that the integration is performed over the region $\rho > \rho_s$. The factor $\sqrt{g'}$ represents the square root of the determinant of the spacetime metric in the coordinates (x'_1, x'_2, x'_3) . The specific definition of the coordinates (x'_1, x'_2, x'_3) is not easy in high genus spacetimes [28]. Fortunately, the exact form of (x'_1, x'_2, x'_3) is not important for this study.

For convenience, we define

$$B_{seed} \equiv B_{in} + B_{wall} \quad (14)$$

as the vacuum decay seed. If there are no wormhole fluctuations, $B = B_{seed}$. This is the characteristic of the conventional Coleman-De Luccia theory [40]. However, if wormhole fluctuations are present, $B_{out} \neq 0$, and thus $B \neq B_{seed}$. To illustrate this result, we initially categorize wormhole fluctuations into three classes. In the first class, both ends of the wormhole are inside the bubble. In the second class, one end of the wormhole is inside the bubble, while the other end is outside the bubble. In the third class, both ends of the wormhole are outside the bubble. Intuitively, boundary wormholes belong to the third class, as depicted in figures 4 and 5.

The size of the bubble is negligible compared to the size of the AdS_3 spacetime. Thus, the predominant wormhole fluctuations belong to the third class. Consequently, the first and second classes can be neglected. Obviously, the third class of wormhole fluctuations affects the volume outside the bubble, thereby impacting the tunneling action B_{out} . In order to calculate B_{out} , recalling that in the case where there are no wormhole fluctuations, the tunneling action B_{out} is defined as [40]

$$B_{out} = \int_{\rho > \bar{\rho}; g=0} d\theta d\varphi d\tau_E \sqrt{g} \mathcal{L}_{eff}(\phi_{bounce}) - \int_{\rho > \bar{\rho}; g=0} d\theta d\varphi d\tau_E \sqrt{g} \mathcal{L}_{eff}(\phi_2). \quad (15)$$

Here, the symbol $\int_{\rho > \bar{\rho}; g=0}$ represents that the integration is performed over the exterior of the bubble. $g = 0$ represents that the genus of the spacetime is zero. The parent universe is spherically symmetric, ensuring that the integral in equation (15) is well defined. On the right hand side of equation (15), the first term and the second term correspond to the bounce solution and the background term, respectively. Outside the bubble, $\phi_{bounce} = \phi_2$. Thus, in the absence of wormhole fluctuations, $B_{out} = 0$.

Taking BWFs into consideration, it is convenient to divide the region outside the bubble into two parts: $\bar{\rho} \leq \rho \leq \rho_s$ and $\rho > \rho_s$, as shown in figure 5. As a result, the tunneling action B_{out} can be written as

$$B_{out} = B_{out}(\bar{\rho} \leq \rho \leq \rho_s) + B_{out}(\rho > \rho_s). \quad (16)$$

Here,

$$B_{out}(\bar{\rho} \leq \rho \leq \rho_s) \equiv \int d\theta d\varphi \int_{\bar{\rho}}^{\rho_s} d\tau_E \sqrt{g} \mathcal{L}_{eff}(\phi_{bounce} = \phi_2) - \int d\theta d\varphi \int_{\bar{\rho}}^{\rho_s} d\tau_E \sqrt{g} \mathcal{L}_{eff}(\phi_2). \quad (17)$$

On the right hand side of equation (16), $B_{out}(\bar{\rho} \leq \rho \leq \rho_s)$ and $B_{out}(\rho > \rho_s)$ represent the tunneling actions in the regions $\bar{\rho} \leq \rho \leq \rho_s$ and $\rho > \rho_s$, respectively. On the right hand side of equation (17), the first term corresponds to the bounce solution, while the second term is the background term. Note that in the region $\bar{\rho} \leq \rho \leq \rho_s$, there are no wormhole fluctuations. Thus, the tunneling action $B_{out}(\bar{\rho} \leq \rho \leq \rho_s) = 0$. This indicates that $B_{out} = B_{out}(\rho > \rho_s)$.

Under the thin wall approximation, the bubble radius $\bar{\rho} \gg 0$ [40]. Thus, when $\rho > \bar{\rho}$, it can be expected that $1/\rho^2 \rightarrow 0$. This indicates that in the region $\bar{\rho} \leq \rho \leq \rho_s$, the effective Lagrangian density of the system can be approximated as

$$\mathcal{L}_{eff}(\phi) = 2V(\phi_2). \quad (18)$$

Equation (18) shows that in the region $\bar{\rho} \leq \rho \leq \rho_s$, the effective Lagrangian density is constant and independent of the spacetime coordinates. In addition, outside the bubble, the scalar field is in the state $V(\phi_2)$. Thus, every point outside the bubble has the same cosmological constant. Therefore, at any point outside the bubble (such as points a , b and c in figure 5), the effective Lagrangian density of the system should be described by equation (18). This implies that $\mathcal{L}_{eff}(\phi) = \mathcal{J}_{eff}(\phi)$. Consequently, the Euclidean action $S_E(\rho > \rho_s)$ in equation (13) becomes

$$S_E(\rho > \rho_s) = 2V(\phi_2) \int_{\rho > \rho_s} dx'_1 dx'_2 dx'_3 \sqrt{g'}. \quad (19)$$

It is clear that the factor $\int_{\rho > \rho_s} dx'_1 dx'_2 dx'_3 \sqrt{g'}$ in equation (19) represents the volume of the region $\rho > \rho_s$.

For convenience, we use $g = n$ to denote that the spacetime genus is equal to n ($n = 0, 1, 2, 3, \dots$). For example, $g = 0$ represents that the spacetime genus is zero. We use $Vol(g = n; \rho > \rho_s)$ to denote the volume of the region $\rho > \rho_s$ in a spacetime with genus $g = n$. Then, the Euclidean action $S_E(\rho > \rho_s)$ in equation (19) can be rewritten as

$$S_E(\rho > \rho_s) = 2V(\phi_2)Vol(g = n; \rho > \rho_s). \quad (20)$$

In equation (20), we have assumed that the spacetime genus produced by BWFs is $g = n$.

Combining equations (4) and (20), the tunneling action $B_{out}(\rho > \rho_s)$ can be written as

$$B_{out}(\rho > \rho_s) = 2V(\phi_2)Vol(g = n; \rho > \rho_s) - 2V(\phi_2)Vol(g = 0; \rho > \rho_s). \quad (21)$$

Here, $Vol(g = 0; \rho > \rho_s)$ represents the volume of the region $\rho > \rho_s$ in the parent universe (the genus of the parent universe is zero). On the right hand side of equation (21), the term $2V(\phi_2)Vol(g = n; \rho > \rho_s)$ represents the Euclidean action of the bounce solution in the region $\rho > \rho_s$, which depends on the volume of the genus $g = n$ spacetime. This term reflects the case where vacuum decay occurs in a genus $g = n$ spacetime. The term $2V(\phi_2)Vol(g = 0; \rho > \rho_s)$ is the background term, corresponding to a solution where the system remains in its initial state. Thus, the background term corresponds to the parent universe. Therefore, it is related to the volume of the parent universe.

We have illustrated that the region $\rho < \bar{\rho}$ is not altered by the third class of wormhole fluctuations (the first and second classes can be neglected). This indicates that

$$Vol(g = n; \rho \leq \rho_s) = Vol(g = 0; \rho \leq \rho_s). \quad (22)$$

Here, $Vol(g = n; \rho \leq \rho_s)$ represents the volume of the region $\rho \leq \rho_s$ in a spacetime with genus $g = n$, while $Vol(g = 0; \rho \leq \rho_s)$ is the corresponding volume in the parent universe. Combining equations (21) and (22), the tunneling action B_{out} can be written as

$$B_{out} = B_{out}(\rho > \rho_s) = 2V(\phi_2)\{Vol(g = n) - Vol(g = 0)\}. \quad (23)$$

In equation (23), $Vol(g = n)$ represents the volume of the AdS_3 spacetime with genus $g = n$, while $Vol(g = 0)$ is the volume of the parent universe.

Both $Vol(g = n)$ and $Vol(g = 0)$ are infinite. Typically, the regularized volume is used to replace these terms [20]. We denote the regularized volume of the AdS_3 spacetime with genus $g = n$ as $Rvol(g = n)$. Then, equation (23) is modified to

$$B_{out} = 2V(\phi_2)\{Rvol(g = n) - Rvol(g = 0)\}. \quad (24)$$

Equation (24) implies that BWFs result in $B_{out} \neq 0$.

In this study, we only focus on physics at zero temperature. Physically, as the temperature (T) of the thermal AdS_3 spacetime ($TAdS_3$) approaches zero, the $TAdS_3$ spacetime transitions into a zero temperature AdS_3 spacetime with a conformal boundary shaped like a cylinder, as shown in figure 2(a). Therefore, it is reasonable to consider that $\lim_{T \rightarrow 0} TAdS_3$ is equivalent to the genus zero parent universe depicted in figure 2(a). Hence, for convenience, we use $\lim_{T \rightarrow 0} TAdS_3$ to define the genus zero parent universe. Furthermore, we denote $V(\phi, T)$ as the scalar potential in the $TAdS_3$ (noting that temperature may influence the scalar potential) and set $\lim_{T \rightarrow 0} V(\phi, T)$ to be equal to the scalar potential $V(\phi)$ in equation (1).

The genus of $TAdS_3$ is one [20]. We use $Rvol_T(g = 1)$ to denote the regularized volume of $TAdS_3$. Then, the term $2V(\phi_2)Rvol(g = 0)$ in equation (24) can be expressed as

$$2V(\phi_2)Rvol(g = 0) = 2 \lim_{T \rightarrow 0} \left(V(\phi_2, T) \cdot Rvol_T(g = 1) \right). \quad (25)$$

Similarly, we use $Rvol_T(g = n + 1)$ to represent the regularized volume of the spacetime where the parent universe is $TAdS_3$ and the genus generated by BWFs is n . And $g = n + 1$ is the total genus of the AdS_3 handlebody. Subsequently, the term $2V(\phi_2)Rvol(g = n)$ in equation (24) can be represented as

$$2V(\phi_2)Rvol(g = n) = 2 \lim_{T \rightarrow 0} \left(V(\phi_2, T) \cdot Rvol_T(g = n + 1) \right). \quad (26)$$

Hence, equation (24) can be rewritten as

$$B_{out} = 2 \lim_{T \rightarrow 0} \left\{ V(\phi_2, T) \cdot \left(Rvol_T(g = n + 1) - Rvol_T(g = 1) \right) \right\}. \quad (27)$$

In equation (27), when $n = 0$, $B_{out} = 0$. This corresponds to the case where there are no wormhole fluctuations.

The regularized volume of the AdS_3 handlebody can be obtained from the regularized Euclidean Einstein-Hilbert action of the AdS_3 spacetime, defined as [13, 20]

$$I_{reg} \equiv -\frac{1}{2} \int dx^3 \sqrt{g}(R - 2\Lambda) + 2 \int dx^2 \sqrt{\gamma}(K - \sqrt{-\Lambda}) + \text{Count.} \quad (28)$$

Here, Λ is the cosmological constant ($\Lambda < 0$), while K and γ represent the trace of the extrinsic curvature and the induced metric on the boundary, respectively. The term *Count.* refers to the counterterm used to remove the logarithmic divergence [20]. A detailed discussion of this counterterm can be found in [13]. The regularized action (28) and the Euclidean Einstein-Hilbert action $-\int dx^3 \sqrt{g}(R/2 - \Lambda)$ correspond to the same dynamical equation.

In [20], Krasnov demonstrated that the regularized action I_{reg} can be simplified as

$$I_{reg} = 2\pi \sqrt{\frac{-1}{\Lambda}} (\ln|k_1| + \ln \rho_2 \rho'_2 \cdots \rho_g \rho'_g), \quad (29)$$

where ρ_i (ρ'_i) represents the radius of the Schottky circle C_i (C'_i), and k_1 is the multiplier of the generator L_1 of the Schottky group $\mathbf{Sch}(L_1, L_2, \dots, L_g)$. Definitions of the Schottky circle, Schottky group, and the multiplier k_1 of the generator L_1 are provided in appendix A. In the case of $g = 1$, the regularized action is $I_{reg} = 2\pi \sqrt{-1/\Lambda} \ln|k_1|$. This is the regularized action of TAdS_3 [20]. Thus, the variable k_1 and the generator L_1 are associated with TAdS_3 . The action of the BTZ black hole can also be represented as the regularized action I_{reg} with $g = 1$ [20]. The distinction between TAdS_3 and the BTZ black hole lies in the fact that, for TAdS_3 , the time circle (a circle where different points on the circle correspond to different times) is non contractible, whereas, for the BTZ black hole, the time circle is contractible [20].

Equation (29) can also be derived from the Takhtajan-Zograf action, which is defined as [13, 20, 47]

$$I_{TZ} = \frac{1}{2} \sqrt{\frac{-1}{\Lambda}} \left\{ \iint_{F_S} \frac{i}{2} dz \wedge d\bar{z} (4\partial_z \psi \partial_{\bar{z}} \psi + \frac{1}{2} e^{2\psi}) + i \int_{C_j} \sum_{j=2}^g (d\bar{z} \psi \frac{\partial_z^2 \bar{L}_j}{\partial_z \bar{L}_j} - dz \psi \frac{\partial_z^2 L_j}{\partial_z L_j}) \right. \\ \left. + \frac{i}{2} \int_{C_j} \sum_{j=2}^g \ln |\partial_z L_j|^2 \frac{\partial_z^2 L_j}{\partial_z L_j} dz + 4\pi \sum_{j=2}^g \ln |(L_j)_{21}|^2 \right\}. \quad (30)$$

Here, I_{TZ} and ψ represent the Takhtajan-Zograf action and the Liouville conformal field, respectively. C_j and F_S represent the Schottky circle and the fundamental domain of

the Schottky group $\mathbf{Sch}(L_1, L_2, \dots, L_g)$ acting on the Riemann sphere \mathbb{S} , respectively. \bar{z} and \bar{L}_j represent the complex conjugate of z and L_j , respectively. $(L_j)_{21}$ refers to the element in the second row and first column of the generator L_j . Equation (80) in appendix A indicates that $(L_j)_{21} = (1 - k_j)/(\sqrt{|k_j|}|\xi_j - \eta_j|)$. Here, ξ_j, η_j and k_j are the attractive fixed point, repelling fixed point and multiplier of the generator L_j , respectively. Detailed explanations of these parameters are provided in appendix A. The Takhtajan-Zograf action corresponds to the action of the Liouville conformal field theory defined on the conformal boundary of the AdS_3 handlebody spacetime. One can also use holographic duality to study wormhole fluctuations and AdS vacuum decay [11, 24, 48–51]. However, this approach is beyond the scope of this work and will not be discussed further.

The relationship between the radius of the Schottky circle and the parameters (ξ_i, η_i, k_i) is given by [52, 53]

$$\rho_i = \rho'_i = \left| \frac{\sqrt{k_i}(\xi_i - \eta_i)}{1 - k_i} \right|. \quad (31)$$

Therefore, the regularized action I_{reg} can be expressed as

$$I_{reg} = 2\pi\sqrt{\frac{-1}{\Lambda}} \left\{ \ln|k_1| + 2\ln \left| \frac{\sqrt{k_2}(\xi_2 - \eta_2)}{1 - k_2} \frac{\sqrt{k_3}(\xi_3 - \eta_3)}{1 - k_3} \dots \frac{\sqrt{k_g}(\xi_g - \eta_g)}{1 - k_g} \right| \right\}. \quad (32)$$

The normalized condition of the Schottky group implies that $\xi_2 = 1$. Equation (32) clearly indicates that the regularized action I_{reg} is a $(6g - 6)$ -variate function in the Schottky space. The variables are $(k_1, \eta_2, k_2, \xi_3, \eta_3, k_3, \dots, \xi_g, \eta_g, k_g)$ with $g \geq 2$. In the case of $g = 1$, the unique variable of I_{reg} is k_1 . The variable k_1 describes the properties of TAdS_3 , while the other variables $(\eta_2, k_2, \xi_3, \eta_3, k_3, \dots, \xi_g, \eta_g, k_g)$ describe the properties of the boundary wormholes.

Recalling that for the TAdS_3 , the relationship between the regularized action and the regularized volume $Rvol_T(g = 1)$ is given by $I_{reg} = -2\Lambda \cdot Rvol_T(g = 1)$. This relationship can be easily extended to any genus AdS_3 spacetime: $I_{reg} = -2\Lambda \cdot Rvol(g = n)$. Therefore, based on equation (32), the regularized volume $Rvol_T(g = n + 1)$ can be

represented as

$$Rvol_T(g = n + 1) = -\frac{\pi}{\Lambda} \sqrt{\frac{-1}{\Lambda}} \left\{ \ln|k_1| + 2\ln \left| \frac{\sqrt{k_2}(1 - \eta_2)}{1 - k_2} \right| \right. \\ \left. + 2\ln \left| \frac{\sqrt{k_3}(\xi_3 - \eta_3)}{1 - k_3} \dots \frac{\sqrt{k_g}(\xi_g - \eta_g)}{1 - k_g} \right| \right\}. \quad (33)$$

The term $-\pi\Lambda^{-1}\sqrt{-\Lambda^{-1}}\ln|k_1|$ in equation (33) represents the regularized volume of TAdS₃.

Assuming that the period matrix of TAdS₃ is $\Pi(1)$. For the genus one handlebody, $\Pi(1)$ corresponds to the modular parameter of the torus (refer to appendix B). Equation (92) in appendix B shows that $2\pi i\Pi(1) = \ln k_1$. Furthermore, the inverse of the temperature ($\frac{1}{T}$) of TAdS₃ is proportional to the imaginary part of $\Pi(1)$ [20, 43]. Therefore, $\frac{1}{T} \propto \ln|k_1|$. Other parameters ($\eta_2, k_2, \xi_3, \eta_3, k_3, \dots, \xi_g, \eta_g, k_g$) are independent of the multiplier k_1 , and thus they are also independent of the temperature T . The term proportional to $\ln|k_1|$ in equation (33) is cancelled by the term $Rvol_T(g = 1)$ in equation (27). Combining equation (33) with this conclusion, equation (27) can be written as

$$B_{out} = -4\pi \sqrt{\frac{-1}{V(\phi_2)}} \left\{ \ln \left| \frac{\sqrt{k_2}(1 - \eta_2)}{1 - k_2} \frac{\sqrt{k_3}(\xi_3 - \eta_3)}{1 - k_3} \dots \frac{\sqrt{k_g}(\xi_g - \eta_g)}{1 - k_g} \right| \right\}. \quad (34)$$

Here, we have used the fact that in the parent universe $\lim_{T \rightarrow 0} \text{TAdS}_3$, the cosmological constant is equal to $V(\phi_2)$ (outside the bubble). Equation (34) indicates that the tunneling action B_{out} is a $(6g - 8)$ -variate function in the Schottky space.

In addition, the third class of wormhole fluctuations is independent of the bounce bubble, meaning it does not affect the vacuum decay seed B_{seed} . Therefore, when calculating the vacuum decay seed B_{seed} , one can simply assume that there are no wormhole fluctuations. Using the method described in reference [40], one can obtain

$$B_{seed} = 4\pi \left\{ V^{-\frac{1}{2}}(\phi_2) \arcsin(\bar{\rho}\sqrt{V(\phi_2)}) - V^{-\frac{1}{2}}(\phi_1) \arcsin(\bar{\rho}\sqrt{V(\phi_1)}) \right. \\ \left. + \bar{\rho}\sqrt{1 - \bar{\rho}^2 V(\phi_2)} - \bar{\rho}\sqrt{1 - \bar{\rho}^2 V(\phi_1)} + \bar{\rho}^2 \mu \right\} \quad (35)$$

with the radius

$$\bar{\rho} = \frac{2\mu}{\sqrt{\mu^4 + \epsilon^2 + 2\mu^2(2V(\phi_2) + \epsilon)}}. \quad (36)$$

Here, $\mu \equiv \int_{\phi_1}^{\phi_2} d\phi \sqrt{2(V(\phi) - V(\phi_2))}$ represents the tension of the domain wall [41, 54]. The detailed derivation of equations (35) and (36) is presented in appendix C.

To sum up, in this section, we generalize the tunneling action to the case where there are BWFs. The main contribution comes from the third class of wormhole fluctuations, which does not affect the vacuum decay seed B_{seed} . The relationship between the total tunneling action B and the vacuum decay seed B_{seed} is given by $B = B_{seed} + B_{out}$. In the absence of wormhole fluctuations, $B_{out} = 0$. When BWFs are present, B_{out} is described by equation (34).

3.2 Representing the tunneling action in the Siegel upper half space

The parameters $(\eta_2, k_2, \xi_3, \eta_3, k_3, \dots, \xi_g, \eta_g, k_g)$ in equation (34) specify the BWFs. To include the contributions from all BWFs (the third class), one needs to integrate over these parameters. However, the Schottky space is not simply connected [20], and different points in the Schottky space may correspond to the same BWFs. This makes it inconvenient to define the integral domain directly in the Schottky space. Instead, we perform the summation of the BWFs in the Siegel upper half space (**Sie**(g)). By using the relationship between the elements of the period matrix and the parameters (ξ_i, η_i, k_i) , the tunneling action can be transformed from the Schottky space to **Sie**(g). Detailed information about the Siegel upper half space and the period matrix is provided in appendix B.

Combining the normalized condition ($\xi_1 = 0, \xi_2 = 1, \eta_1 = \infty$) of the Schottky group and equation (93) in appendix B, one can obtain

$$\eta_2 = \exp(-2\pi i \Pi(g)_{12}), \quad (37)$$

$$\xi_j = \eta_j \exp(2\pi i \Pi(g)_{1j}), \quad (38)$$

and

$$2\pi i \Pi(g)_{2j} = \ln \frac{(\eta_2 - \eta_j)(1 - \xi_j)}{(\eta_2 - \xi_j)(1 - \eta_j)}. \quad (39)$$

In equations (37)-(40), $\Pi(g)_{ij}$ denotes the element of the period matrix (refer to appendix B).

Substituting equations (37) and (38) into equation (39), one can obtain the relationship between the repelling fixed point η_j and the elements of the period matrix

as

$$\eta_j = \frac{-\Delta_{2j} \pm \sqrt{\Delta_{2j}^2 - 4\Delta_{1j}\Delta_{3j}}}{2\Delta_{1j}}. \quad (40)$$

Here, the symbol “ \pm ” corresponds to two different results. In the later, we will show that only one of the results is meaningful in our model (see appendix D). The terms Δ_{1j} , Δ_{2j} , and Δ_{3j} are defined as follows:

$$\Delta_{1j} \equiv \exp(2\pi i \Pi(g)_{2j}) - \exp(2\pi i \Pi(g)_{1j}), \quad (41)$$

$$\begin{aligned} \Delta_{2j} \equiv & 1 - \exp(2\pi i \Pi(g)_{2j}) \exp(-2\pi i \Pi(g)_{12}) - \exp(2\pi i \Pi(g)_{1j}) \exp(2\pi i \Pi(g)_{2j}) \\ & + \exp(-2\pi i \Pi(g)_{12}) \exp(2\pi i \Pi(g)_{1j}), \end{aligned} \quad (42)$$

$$\Delta_{3j} \equiv \exp(2\pi i \Pi(g)_{2j}) \exp(-2\pi i \Pi(g)_{12}) - \exp(-2\pi i \Pi(g)_{12}). \quad (43)$$

Equation (40) is the representation of the repelling fixed point η_j in the space $\mathbf{Sie}(g)$.

Equation (92) in appendix B indicates that $k_i = \exp(2\pi i \Pi(g)_{ii})$. Using this result and incorporating equations (38) and (40) into equation (34), the tunneling action B_{out} becomes

$$\begin{aligned} B_{out} = & \frac{-4\pi}{\sqrt{-V(\phi_2)}} \left\{ \sum_{j=2}^g \ln \left| \frac{\exp(\pi i \Pi(g)_{jj})(\exp(2\pi i \Pi(g)_{1j}) - 1)}{1 - \exp(2\pi i \Pi(g)_{jj})} \right| \right. \\ & \left. + \sum_{j=2}^g \ln \left| \frac{-\Delta_{2j} \pm \sqrt{\Delta_{2j}^2 - 4\Delta_{1j}\Delta_{3j}}}{2\Delta_{1j}} \right| \right\}. \end{aligned} \quad (44)$$

Equations (40)-(44) show that in the space $\mathbf{Sie}(g)$, the tunneling action B_{out} depends on the set of parameters $(\Pi(g)_{22}, \Pi(g)_{33}, \dots, \Pi(g)_{gg}; \Pi(g)_{12}, \Pi(g)_{13}, \dots, \Pi(g)_{1g}; \Pi(g)_{23}, \Pi(g)_{24}, \dots, \Pi(g)_{2g})$. These parameters fully specify the BWFs.

In our setup, the generator L_1 of the Schottky group $\mathbf{Sch}(L_1, L_2, \dots, L_g)$, the multiplier k_1 , and the parameter $\Pi(g)_{11}$ ($2\pi i \Pi(g)_{11} = \ln k_1$) all correspond to the parent universe $\lim_{T \rightarrow 0} \text{TAdS}_3$. Other generators L_i ($i \neq 1$) correspond to the wormholes. Thus, in equation (44), $j \geq 2$. The maximum value of j being g implies that the genus produced by the BWFs is $g - 1$. The element $\Pi(g)_{1j}$ ($j \neq 1$) should be interpreted as the interaction between the parent universe $\lim_{T \rightarrow 0} \text{TAdS}_3$ and wormhole j . And the element $\Pi(g)_{ij}$ ($i, j \neq 1; i \neq j$) should be interpreted as the interaction between wormholes i and j (refer to appendix B or reference [53]).

To simplify equation (44), we denote $\Pi(g) = X + iY$, where X and Y are real symmetric $g \times g$ matrices. Define

$$\Xi(\phi_2) \equiv 2\pi \sqrt{\frac{-1}{V(\phi_2)}}. \quad (45)$$

Under the dilute wormhole gas approximation [53, 55] (refer to appendix B), equation (44) can be simplified to

$$\begin{aligned} B_{out} = & -\Xi(\phi_2)(g-1)\ln\left(1 + \exp(4\pi Y_{12}) - 2\cos(2\pi X_{12})\exp(2\pi Y_{12})\right) \\ & - \Xi(\phi_2) \sum_{j=2}^g \left\{ -2\pi Y_{jj} - \ln\left(1 + \exp(-4\pi Y_{jj}) - 2\cos(2\pi X_{jj})\exp(-2\pi Y_{jj})\right) \right. \\ & \left. + \ln\left(1 + \exp(-4\pi Y_{1j}) - 2\cos(2\pi X_{1j})\exp(-2\pi Y_{1j})\right) \right\}. \end{aligned} \quad (46)$$

The derivation of equation (46) is presented in appendix D. Equation (46) shows that the tunneling action B_{out} is a function of the set of variables $(X_{22}, X_{33}, \dots, X_{gg}, Y_{22}, Y_{33}, \dots, Y_{gg}, X_{12}, X_{13}, \dots, X_{1g}, Y_{12}, Y_{13}, \dots, Y_{1g})$.

The tunneling action B_{out} in equation (46) is still complicated. In appendix D, we have demonstrated that under the dilute wormhole gas approximation, the interactions between different wormholes are very weak, giving justification to ignore them. To further simplify equation (46), we consider the case where the interactions between the parent universe and the wormholes are also small. Specifically, we focus on the case where

$$\Pi(g)_{ij} \quad (i, j \neq 1; i \neq j) \ll \Pi(g)_{1j} \quad (j \neq 1) \ll 1. \quad (47)$$

This implies that all non-diagonal elements of the period matrix are small, and the interactions between different wormholes are significantly weaker than those between the parent universe and the wormholes.

Under condition (47), it is reasonable to neglect the interactions between different wormholes and approximate the terms related to the interactions between the parent universe and the wormholes to the first order. Thus, $\cos(2\pi X_{1j}) \approx 1$ and $\exp(\pm 2\pi Y_{1j}) \approx 1 \pm 2\pi Y_{1j}$. Using these approximations, equation (46) can be simplified to

$$B_{out} = 2\Xi(\phi_2) \sum_{j=2}^g \left\{ \pi Y_{jj} - \ln(2\pi Y_{1j}) \right\} - 2\Xi(\phi_2)(g-1)\ln(2\pi Y_{12}). \quad (48)$$

The element $\Pi_{1j}(j \neq 1)$ represents the interaction between the parent universe and wormhole “ j ”. Equation (48) indicates that the tunneling action B_{out} is independent of the variable X_{1j} . Thus, under condition (47), $Y_{1j}(j \neq 1)$ can be used to describe the coupling strength between the parent universe and wormhole “ j ”. Equation (48) expresses the tunneling action B_{out} in the space $\mathbf{Sie}(g)$. Note that the vacuum decay seed B_{seed} is independent of the elements of the period matrix. Therefore, by representing B_{out} in the space $\mathbf{Sie}(g)$, the total tunneling action B is also represented in the space $\mathbf{Sie}(g)$.

4 Integration for the non-equivalent boundary wormhole fluctuations

In the Coleman-De Luccia theory, the vacuum decay rate $e^{-B_{seed}}$ corresponds to scenarios without wormhole fluctuations. However, during the vacuum decay process, spacetime can fluctuate to generate one or more wormholes. Various fluctuations correspond to different vacuum decay processes. To calculate the total vacuum decay rate, all possible vacuum decay processes must be taken into account. Different BWFs are represented by distinct handlebodies. Thus, one needs to integrate over the non-equivalent handlebodies. The vacuum decay rate associated with a specific type of boundary wormhole fluctuation is $e^{-(B_{seed}+B_{out})}$, where B_{out} is given by equation (48). Therefore, the total vacuum decay rate defined by equation (5) should be

$$\Gamma_{tot} = e^{-B_{seed}} + \sum_{g=2}^{\infty} \int_{\mathfrak{F}(g)} e^{-(B_{seed}+B_{out})} d\sigma(g), \quad (49)$$

where $\mathfrak{F}(g)$ and $d\sigma(g)$ represent the integral domain and the integral measure, respectively.

In equation (49), the first term on the right hand side represents the vacuum decay rate for the scenario without wormhole fluctuations. The second term accounts for the contributions from BWFs. The parameter g starts at $g = 2$ because $g = 2$ represents the genus produced by the BWFs as one. The vacuum decay seed B_{seed} is given by equation (35). The total tunneling action $B_{seed} + B_{out}$ is determined by equations (35) and (48).

In the integral domain $\mathfrak{F}(g)$, each point represents a different handlebody spacetime. In other words, each point in $\mathfrak{F}(g)$ corresponds to a different boundary wormhole fluctuation. To elucidate the integral domain $\mathfrak{F}(g)$, it is crucial to note that in the space $\mathbf{Sie}(g)$, when two period matrices are associated by a modular transformation, they describe conformally equivalent Riemann surfaces Σ_g (Σ_g denotes the closed Riemann surface of genus g , see appendix A for more details). The modular transformation between two period matrices $\Pi(g)^{(a)}$ and $\Pi(g)^{(b)}$ is defined as [56]

$$\Pi(g)^{(a)} = \frac{A\Pi(g)^{(b)} + B}{C\Pi(g)^{(b)} + D}, \quad (50)$$

where A, B, C, D are $g \times g$ matrices. Each element of these matrices is an integer. These matrices must satisfy the conditions $AB^T = BA^T$, $CD^T = DC^T$, and $AD^T - BC^T = \mathbb{I}_g$ [29, 31], where \mathbb{I}_g represents the $g \times g$ identity matrix and M^T denotes the transpose of the matrix M .

The set of all modular transformations forms the modular group $\text{Sp}(2g, \mathbb{Z})$. This group has two generators [57]

$$G(g)^{(1)} = \begin{pmatrix} \mathbb{I}_g & S \\ 0 & \mathbb{I}_g \end{pmatrix}, \quad G(g)^{(2)} = \begin{pmatrix} 0 & \mathbb{I}_g \\ -\mathbb{I}_g & 0 \end{pmatrix}. \quad (51)$$

Here, S is an arbitrary $g \times g$ symmetric integer matrix. Every element of the modular group $\text{Sp}(2g, \mathbb{Z})$ can be generated by these two generators. Equations (50) and (51) show that the generator $G(g)^{(1)}$ acts on the period matrix $\Pi(g)$ as $\Pi(g) \rightarrow \Pi(g) + S$, while the generator $G(g)^{(2)}$ acts on $\Pi(g)$ as $\Pi(g) \rightarrow -\Pi(g)^{-1}$. Some researchers may claim that the modular group $\text{Sp}(2g, \mathbb{Z})$ has three generators [57, 58]. However, an additional generator can be generated by the generators $G(g)^{(1)}$ and $G(g)^{(2)}$ [57]. Therefore, it is sufficient to consider the generators $G(g)^{(1)}$ and $G(g)^{(2)}$.

The simplest case is the genus one closed Riemann surface Σ_1 . In this case, the period matrix $\Pi(1)$ is the modular parameter of the torus. The related modular group is $\text{Sp}(2, \mathbb{Z})$, which is generated by the following generators [59–61]

$$G(1)^{(1)} = \begin{pmatrix} 1 & 1 \\ 0 & 1 \end{pmatrix}, \quad G(1)^{(2)} = \begin{pmatrix} 0 & 1 \\ -1 & 0 \end{pmatrix}. \quad (52)$$

It is straightforward to verify that $G(1)^{(1)}$ and $G(1)^{(2)}$ satisfy the multiplication rules $(G(1)^{(2)})^2 = (G(1)^{(2)}G(1)^{(1)})^3 = \mathbb{I}_2$ [59]. The generator $G(1)^{(1)}$ generates the Dehn twist

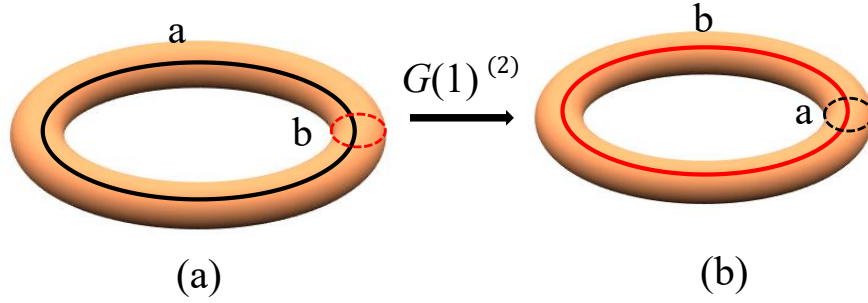


Figure 6: The transformation $G(1)^{(2)}$ transforms the torus (a) into the torus (b). In figures (a) and (b), the tori have two dimensions a and b . The transformation $G(1)^{(2)}$ exchanges the two dimensions a and b .

of the torus ($\Pi(1) \rightarrow \Pi(1) + 1$). The transformations generated by $G(1)^{(2)}$ exchange the two dimensions of the torus ($\Pi(1) \rightarrow -1/\Pi(1)$) [42], as shown in figure 6. If the torus $\Pi(1)$ represents a two dimensional spacetime, then the torus $-1/\Pi(1)$ also represents a two dimensional spacetime. Mathematically, the tori $\Pi(1)$ and $-1/\Pi(1)$ share the same conformal structure. However, physically, they represent different spacetimes due to differences in their time circles. Filling their interiors results in two non-equivalent three-dimensional handlebody spacetimes. Thus, the transformation $G(1)^{(2)}$ may alter the properties of the handlebody spacetime. A specific example is that the modular transformation $G(1)^{(2)}$ converts the TAdS₃ spacetime into the BTZ black hole [24].

The initial (or final) state defined in the TAdS₃ spacetime and the BTZ black hole corresponds to a spatial slice. The spatial slice of TAdS₃ is topologically distinct from that of the BTZ black hole. This indicates that one cannot define the same initial (or final) state in the TAdS₃ spacetime and the BTZ black hole. At least, the topological structures of the initial (or final) state defined in these two types of spacetimes are different. More generally, if the modular transformation $G(1)^{(2)}$ exchanges the time and space dimensions of a handlebody spacetime, it becomes impossible to define the same initial (or final) state in the spacetimes associated by the transformation $G(1)^{(2)}$. Therefore, specifying an initial state implies selecting a specific spacetime from the set of spacetimes associated with the modular transformation $G(1)^{(2)}$.

The generators $G(g)^{(1)}$ and $G(g)^{(2)}$ are generalizations of the generators $G(1)^{(1)}$ and $G(1)^{(2)}$, respectively. Similar to the case of $G(1)^{(2)}$, one can easily show that $(G(g)^{(2)})^2 = \mathbb{I}_{2g}$. This implies that the modular transformations generated by $G(g)^{(2)}$,

when acting on a genus g handlebody spacetime, can only result in one other distinct spacetime. The generator $G(g)^{(2)}$ acts on the period matrix as $\Pi(g) \rightarrow -\Pi(g)^{-1}$.

Under condition (47), the period matrix $\Pi(g)$ can be written as $\Pi(g) = \bigoplus_{i=1}^g \Pi(g)_{ii} + o(\Pi(g)_{ij})$, where $o(\Pi(g)_{ij})$ is a small term determined by the off-diagonal elements of Π . Utilizing the formula [62]

$$(A - B)^{-1} = A^{-1} + A^{-1}BA^{-1} + A^{-1}BA^{-1}BA^{-1} + \dots \quad (53)$$

the inverse of the period matrix $-\Pi(g)^{-1}$ can be written as

$$\begin{aligned} -\Pi(g)^{-1} = & -\left(\bigoplus_{i=1}^g \Pi(g)_{ii}^{-1}\right) \left\{ \mathbb{I}_g - o(\Pi(g)_{ij}) \left(\bigoplus_{i=1}^g \Pi(g)_{ii}^{-1}\right) \right. \\ & \left. + o(\Pi(g)_{ij}) \left(\bigoplus_{i=1}^g \Pi(g)_{ii}^{-1}\right) o(\Pi(g)_{ij}) \left(\bigoplus_{i=1}^g \Pi(g)_{ii}^{-1}\right) + \dots \right\}. \end{aligned} \quad (54)$$

The dominant term on the right hand side of equation (54) is $-\bigoplus_{i=1}^g \Pi(g)_{ii}^{-1}$. Hence, the leading terms of $\Pi(g)$ and $-\Pi(g)^{-1}$ are $\bigoplus_{i=1}^g \Pi(g)_{ii}$ and $-\bigoplus_{i=1}^g \Pi(g)_{ii}^{-1}$, respectively. Both $\bigoplus_{i=1}^g \Pi(g)_{ii}$ and $-\bigoplus_{i=1}^g \Pi(g)_{ii}^{-1}$ represent multiple disconnected spacetimes.

We have demonstrated that it is impossible to define the same initial (or final) state in the spacetimes $\Pi(g)_{ii}$ and $-\Pi(g)_{ii}^{-1}$. Thus, one also cannot define the same initial (or final) state in the spacetimes $\bigoplus_{i=1}^g \Pi(g)_{ii}$ and $-\bigoplus_{i=1}^g \Pi(g)_{ii}^{-1}$. Therefore, it is reasonable to infer that one cannot define the same initial (or final) state in the handlebody spacetimes $\Pi(g)$ and $-\Pi(g)^{-1}$. In our model, the initial state is specified as the spatial slice at the initial time of the parent universe $\lim_{T \rightarrow 0} \text{TAdS}_3$. Assuming that this initial state can be defined in the spacetime $\Pi(g)$, then in the spacetime $-\Pi(g)^{-1}$, one can not define the same initial state. Therefore, the spacetime $-\Pi(g)^{-1}$ should not be included in the integral domain $\mathfrak{F}(g)$. Consequently, specifying the initial state breaks the modular symmetry $\text{Sp}(2g, \mathbb{Z})$.

We denote the group freely generated by the generator $G(g)^{(1)}$ as \mathbf{P} . The group \mathbf{P} is a subgroup of $\text{Sp}(2g, \mathbb{Z})$. One can easily verify that the modular transformations in the group \mathbf{P} act trivially on the tunneling action B_{out} and the vacuum decay seed B_{seed} . Therefore, in our model, the spacetimes associated by modular transformations in the group \mathbf{P} are physically equivalent. In studies of the partition function of high genus

AdS₃ spacetimes, other researchers have also suggested that the spacetimes associated with the group \mathbf{P} are equivalent [11, 29, 31, 63]. Considering this, when summing over different BWFs, one does not need to account for the spacetimes connected by modular transformations which are generated by $G(g)^{(1)}$ and $G(g)^{(2)}$. Since any element of the modular group $\text{Sp}(2g, \mathbb{Z})$ can be generated by $G(g)^{(1)}$ and $G(g)^{(2)}$, modular transformations in the modular group $\text{Sp}(2g, \mathbb{Z})$ do not need to be included in this summation.

The fundamental domain of the modular group $\text{Sp}(2g, \mathbb{Z})$ in the space $\mathbf{Sie}(g)$ can be expressed as $\mathbf{Sie}(g)/\text{Sp}(2g, \mathbb{Z})$. Any point in $\mathbf{Sie}(g)/\text{Sp}(2g, \mathbb{Z})$ cannot be associated with another point by transformations in the modular group $\text{Sp}(2g, \mathbb{Z})$. Moreover, any point in the space $\mathbf{Sie}(g)$ can be mapped to a single point in $\mathbf{Sie}(g)/\text{Sp}(2g, \mathbb{Z})$. The fundamental domain $\mathbf{Sie}(g)/\text{Sp}(2g, \mathbb{Z})$ is a connected subspace of $\mathbf{Sie}(g)$. Any period matrix outside the fundamental domain $\mathbf{Sie}(g)/\text{Sp}(2g, \mathbb{Z})$ can always be associated with a unique period matrix inside it. Thus, when summing over different BWFs, one only needs to consider the period matrices within the fundamental domain $\mathbf{Sie}(g)/\text{Sp}(2g, \mathbb{Z})$. In other words, spacetimes outside the fundamental domain $\mathbf{Sie}(g)/\text{Sp}(2g, \mathbb{Z})$ should not be included in the integral domain $\mathfrak{F}(g)$. Furthermore, handlebodies within the fundamental domain $\mathbf{Sie}(g)/\text{Sp}(2g, \mathbb{Z})$ that do not satisfy condition (47) should also be excluded from the integral domain $\mathfrak{F}(g)$. Therefore, the integral domain $\mathfrak{F}(g)$ is a subspace of the fundamental domain $\mathbf{Sie}(g)/\text{Sp}(2g, \mathbb{Z})$.

It is well known that the fundamental domain of the modular group $\text{Sp}(2, \mathbb{Z})$ in the space $\mathbf{Sie}(1)$ is determined by the equation [64]

$$\mathbf{Sie}(1)/\text{Sp}(2, \mathbb{Z}) = \left\{ \begin{array}{l} |\Pi(1)| \geq 1 \\ |X| = |\text{Re}(\Pi(1))| \leq \frac{1}{2} \end{array} \right. . \quad (55)$$

Here, $\text{Re}(\Pi(1))$ represents the real part of the period matrix $\Pi(1)$. The shaded region in figure 7 represents the fundamental domain $\mathbf{Sie}(1)/\text{Sp}(2, \mathbb{Z})$. It is a two dimensional connected space. No two points within the shaded region (excluding boundary points) can be associated by modular transformation in the group $\text{Sp}(2, \mathbb{Z})$. Consequently, different points in the shaded region correspond to different handlebody spacetimes, and each point satisfies equation (55). The boundaries of the fundamental domain $\mathbf{Sie}(1)/\text{Sp}(2, \mathbb{Z})$ are defined by the equations $X = \pm 0.5$ and $X^2 + Y^2 = 1$ with $Y > 0$.

In the case where the BWFs produce only one wormhole, the period matrix is given

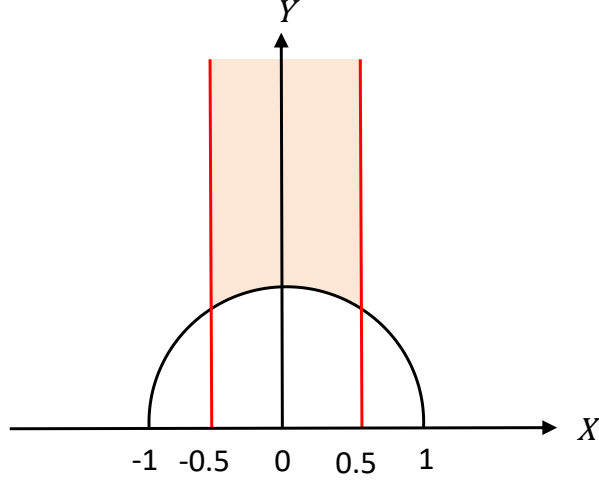


Figure 7: The fundamental domain of the modular group $\text{Sp}(2, \mathbb{Z})$ in the Siegel upper half space $\mathbf{Sie}(1)$. The shaded region represents the fundamental domain $\mathbf{Sie}(1)/\text{Sp}(2, \mathbb{Z})$. X and Y represent the real part and imaginary part of the period matrix $\Pi(1)$, respectively. The equations of the red lines are $X = \pm 0.5$, and the equation of the black curve is $X^2 + Y^2 = 1$ with $Y > 0$. The intersections of the black curve and the red lines are $(\pm 0.5, \frac{\sqrt{3}}{2})$.

by

$$\Pi(2) = \begin{pmatrix} \Pi(2)_{11} & \Pi(2)_{12} \\ \Pi(2)_{21} & \Pi(2)_{22} \end{pmatrix}. \quad (56)$$

Here, $\Pi(2)_{11}$ and $\Pi(2)_{22}$ correspond to the parent universe $\lim_{T \rightarrow 0} \text{TAdS}_3$ and the wormhole, respectively. The term $\Pi(2)_{12} = \Pi(2)_{21}$ represents the interaction between the parent universe and the wormhole. The temperature of the parent universe being zero implies that $\Pi(2)_{11} = \infty$. When the interaction $\Pi(2)_{12} = 0$, the period matrix simplifies to $\Pi(2) = \Pi(2)_{11} \oplus \Pi(2)_{22}$, indicating that the parent universe and the wormhole are disconnected. In this case, the wormhole degenerates into a genus one universe (a solid torus). Various points in the shaded region of figure 7 represent different genus one universes.

When there is a small interaction between the parent universe and the wormhole, the period matrix (56) can be expressed as $\Pi(2) = \Pi(2)_{11} \oplus \Pi(2)_{22} + o(\Pi(2)_{12})$, where $o(\Pi(2)_{12})$ is a small term determined by the interaction $\Pi_{12}(2)$. The predominant part of the period matrix $\Pi(2)$ is $\Pi(2)_{11} \oplus \Pi(2)_{22}$. Since the interaction is small, its impact on the properties of the period matrix $\Pi(2)$ is small. Therefore, it can be anticipated that within the fundamental domain $\mathbf{Sie}(2)/\text{Sp}(4, \mathbb{Z})$, the value range of the parameter

$\Pi(2)_{22}$ can be expressed as

$$\begin{cases} |\Pi(2)_{22}| \geq 1 + \delta_1 \\ |\text{Re}(\Pi(2)_{22})| \leq \frac{1}{2} + \delta_2 \end{cases} \quad (57)$$

Here, δ_1 and δ_2 represent the influence of the interaction $\Pi(2)_{12}$. For any genus g , the fundamental domain $\mathbf{Sie}(g)/\text{Sp}(2g, \mathbb{Z})$ satisfies the condition $|X_{ij}| \leq \frac{1}{2}$ [57], which implies $\delta_2 = 0$. Since $o(\Pi(2)_{12})$ is small, one can expect that δ_1 is also small. Therefore, equation (55) can still approximately represent the value range of the parameter $\Pi(2)_{22}$ within the fundamental domain $\mathbf{Sie}(2)/\text{Sp}(4, \mathbb{Z})$.

A small $\Pi(2)_{12}$ implies that both X_{12} and Y_{12} are small. Denoting the upper bounds of X_{12} and Y_{12} as α and β (meaning that if $X_{12} > \alpha$ or $Y_{12} > \beta$, condition (47) will break down), respectively. Then the ranges of X_{12} and Y_{12} are $|X_{12}| < \alpha$ ($\alpha > 0$) and $0 \leq Y_{12} \leq \beta$, respectively. Without the restriction of condition (47), $\alpha = \frac{1}{2}$ [57]. The minimum value of Y_{12} being greater than zero arises from the non-negativity of the imaginary part of any element in the space $\mathbf{Sie}(g)$. For convenience, we define $\mathfrak{D} \equiv \{(x, y) \mid -\alpha < x < \alpha; 0 \leq y \leq \beta\}$. Based on these conclusions, when $\Pi(2)_{12}$ is small, the integral domain $\mathfrak{F}(2)$ should be selected as $\mathfrak{F}(2) = (\mathbf{Sie}(1)/\text{Sp}(2, \mathbb{Z})) \otimes \mathfrak{D}$. Points in $\mathbf{Sie}(1)/\text{Sp}(2, \mathbb{Z})$ represent various boundary wormholes, while points in \mathfrak{D} represent different couplings between the wormhole and the parent universe.

Under the dilute wormhole gas approximation, different boundary wormholes are independent of each other. Each wormhole corresponds to an integral domain $\mathfrak{F}(2)$. Therefore, the integral domain $\mathfrak{F}(g)$ should be

$$\mathfrak{F}(g) = \bigotimes_{j=2}^g \mathfrak{F}(2) = \bigotimes_{j=2}^g \left((\mathbf{Sie}(1)/\text{Sp}(2, \mathbb{Z})) \otimes \mathfrak{D} \right). \quad (58)$$

Combining equations (55) and (58), one can show that equation (58) can be written as

$$\mathfrak{F}(g) = \begin{cases} |X_{jj}| \leq \frac{1}{2} \\ Y_{jj} \geq (1 - X_{jj}^2)^{\frac{1}{2}} \\ |X_{1j}| \leq \alpha \\ 0 \leq Y_{1j} \leq \beta \end{cases}, \quad j = 2, 3, \dots, g. \quad (59)$$

The parameters α and β are subject to two conditions. The first condition is that equation (47) must not be violated. The second condition is that the integral domain $\mathfrak{F}(g)$ must be a subspace of the fundamental domain $\mathbf{Sie}(g)/\text{Sp}(2g, \mathbb{Z})$.

Equation (59) is derived under condition (47). Utilizing equations (47) and (92) (refer to appendix B), one can show that

$$|k_j| = \exp(-2\pi Y_{jj}) \leq 0.0043. \quad (60)$$

Thus, under condition (47), it is sufficient to approximate the Schottky group $\mathbf{Sch}(L_1, L_2, \dots, L_g)$ to the first order of the multiplier k_j .

For the integral measure $d\sigma(g)$, equation (59) implies that the integral variables are $(X_{22}, X_{33}, \dots, X_{gg}, Y_{22}, Y_{33}, \dots, Y_{gg}, X_{12}, X_{13}, \dots, X_{1g}, Y_{12}, Y_{13}, \dots, Y_{1g})$. Thus, the most general form of $d\sigma(g)$ is

$$\begin{aligned} d\sigma(g) = & \mathfrak{G}(X_{22}, \dots, Y_{1g}) dX_{22} dX_{33} \cdots dX_{gg} dY_{22} dY_{33} \cdots dY_{gg} \\ & \times dX_{12} dX_{13} \cdots dX_{1g} dY_{12} dY_{13} \cdots dY_{1g}. \end{aligned} \quad (61)$$

Here, $\mathfrak{G}(X_{22}, \dots, Y_{1g})$ represents the determinant of the metric defined in the space $(X_{22}, X_{33}, \dots, X_{gg}, Y_{22}, Y_{33}, \dots, Y_{gg}, X_{12}, X_{13}, \dots, X_{1g}, Y_{12}, Y_{13}, \dots, Y_{1g})$. The path integral typically corresponds to the Lebesgue measure in the configuration space. Following this reasoning, one may consider setting $\mathfrak{G}(X_{22}, \dots, Y_{1g}) = 1$. As a result, the integral measure (61) becomes

$$\begin{aligned} d\sigma(g) = & dX_{22} dX_{33} \cdots dX_{gg} dY_{22} dY_{33} \cdots dY_{gg} \\ & \times dX_{12} dX_{13} \cdots dX_{1g} dY_{12} dY_{13} \cdots dY_{1g}. \end{aligned} \quad (62)$$

The integral measure (62) is the simplest one. Equation (62) implies that different handlebodies correspond to the same amplitude in the real-time path integral.

In the space $\mathbf{Sie}(g)$, the modular invariant uniquely determines the integral measure up to a constant factor [57]. If the theory is modular invariant, the modular invariant integral measure should be used. However, since our model lacks modular invariance, one should not determine the function $\mathfrak{G}(X_{22}, \dots, Y_{1g})$ based on modular symmetry. Additionally, the primary qualitative results of this study are independent of the specific form of the integral measure (as will be demonstrated later). Therefore, for convenience, we choose the simplest integral measure given by equation (62).

Equation (61) and (62) show that the dimension of the integral space $(X_{22}, X_{33}, \dots, X_{gg}, Y_{22}, Y_{33}, \dots, Y_{gg}, X_{12}, X_{13}, \dots, X_{1g}, Y_{12}, Y_{13}, \dots, Y_{1g})$ is $4g - 4$. Thus, the dimension of the integral space differs from that of the dimension of the Schottky space and the

Teichmüller space of the Riemann surface Σ_g (refer to appendix A). This result arises from two main reasons. Firstly, we only focus on BWFs that satisfy condition (47). Any spacetime configurations failing to meet this criterion fall outside the scope of our analysis. Secondly, the parameters X_{11} and Y_{11} are associated with the parent universe. When summing over the BWFs, these parameters should not serve as integral variables.

We pointed out that without restricting the interactions between the parent universe and the wormholes to be small, equations (41)-(44) indicate that the tunneling action B_{out} becomes a function of the variables $(X_{22}, X_{33}, \dots, X_{gg}, Y_{22}, Y_{33}, \dots, Y_{gg}, X_{12}, X_{13}, \dots, X_{1g}, Y_{12}, Y_{13}, \dots, Y_{1g}, X_{23}, X_{24}, \dots, X_{2g}, Y_{23}, Y_{24}, \dots, Y_{2g})$. In such a scenario, the dimension of the integral space increases to $6g - 8$. Thus, after subtracting the dimensions related to the multiplier k_1 , the dimension of the Schottky space of the Riemann surface Σ_g matches that of the integral space.

To sum up, we show that specifying the initial state breaks the modular symmetry of the model. The integral domain $\mathfrak{F}(g)$ is a subspace of the fundamental domain $\mathbf{Sie}(g)/\mathrm{Sp}(2g, \mathbb{Z})$. Under condition (47), the integral domain $\mathfrak{F}(g)$ can be selected as (59). Using equations (49), (59), and (62), one can complete the summation over physically non-equivalent BWFs. Although the parameters α and β in equation (59) remain unspecified, we will show that their precise values are irrelevant to the qualitative results.

5 The tunneling rate

5.1 Boundary wormhole creation rate

Generally, up to the leading order of the WKB approximation, the quantum tunneling rate is equal to the tunneling probability [65–67]. Thus, in the semiclassical region, the tunneling rate from the initial state $|i\rangle$ to the final state $|f\rangle$ is given by

$$\exp\left\{-2\left(S_E(|i\rangle \rightarrow |f\rangle) - S_E(|i\rangle)\right)\right\}. \quad (63)$$

Here, $S_E(|i\rangle \rightarrow |f\rangle)$ represents the Euclidean action of the instanton trajectory $|i\rangle \rightarrow |f\rangle$. The instanton trajectory is the solution to the Euclidean Euler-Lagrange dynamical equation. And $S_E(|i\rangle)$ represents the Euclidean action of the process in which the

system remains in the initial state $|i\rangle$. One can check that in the Coleman-De Luccia theory, the factor $e^{-B_{seed}}$ exhibits a similar structure to equation (63).

Comparing equations (15), (24), (27), and (63), it can be observed that the factor $e^{-B_{out}}$ has a similar structure to equation (63). The factor $\lim_{T \rightarrow 0} V(\phi_2, T) Rvol_T(g = n+1)$ in equation (27) represents the regularized Euclidean action of the process in which the BWFs produce $g-1$ wormholes. Therefore, the factor $e^{-B_{out}}$ should be interpreted as the rate to create the genus $g-1$ configuration $(\Pi(g)_{22}, \Pi(g)_{33}, \dots, \Pi(g)_{gg}, \Pi(g)_{12}, \Pi(g)_{13}, \dots, \Pi(g)_{1g})$. Consequently, the total tunneling rate from the genus zero AdS_3 state to the genus $g-1$ AdS_3 state is

$$\Gamma(g-1) = \int_{\mathfrak{F}(g)} e^{-B_{out}} d\sigma(g). \quad (64)$$

The integral domain $\mathfrak{F}(g)$ and the tunneling action B_{out} are given by equations (59) and (48), respectively. The integral measure $d\sigma(g)$ is given by equation (62).

In equation (64), various boundary wormholes (including both microscopic and macroscopic wormholes) are integrated. However, equation (24) shows that a larger wormhole volume corresponds to a larger tunneling action B_{out} . Thus, the tunneling rate $e^{-B_{out}}$ for a larger boundary wormhole is smaller, indicating that larger boundary wormholes are more difficult to create. Consequently, microscopic BWFs are dominant.

In our model, $\Pi(2)_{11} = \infty$. Thus, the genus one spacetime can be parameterized by the parameters $(\Pi(2)_{22}, \Pi(2)_{12})$. This type of spacetime represents a fluctuation process of a boundary wormhole. Setting $g = 2$ in equation (48), one can obtain that the rate of creating the configuration $(\Pi(2)_{22}, \Pi(2)_{12})$:

$$\Gamma(\Pi(2)_{22}, \Pi(2)_{12}) = \exp\{-2\pi\Xi(\phi_2)Y_{22}\}(2\pi Y_{12})^{4\Xi(\phi_2)}. \quad (65)$$

Equation (65) shows that the rate $\Gamma(\Pi(2)_{22}, \Pi(2)_{12})$ depends on the parameters $V(\phi_2)$, Y_{22} and Y_{12} . $V(\phi_2)$ is the cosmological constant, and the parameter Y_{12} represents the coupling strength between the parent universe and the wormhole.

To illustrate the meaning of the parameter Y_{22} , we consider the limit as Y_{12} approaches zero. In this scenario, the wormhole becomes a torus $\Pi(2)_{22}$ and is disconnected from the parent universe. The lattice $L(1, \Pi(2)_{22}) \equiv \{m + n\Pi(2)_{22} \mid m, n \in \mathbb{Z}\}$ in the complex plane \mathbb{C} can be used to represent the torus [42]. By connecting the

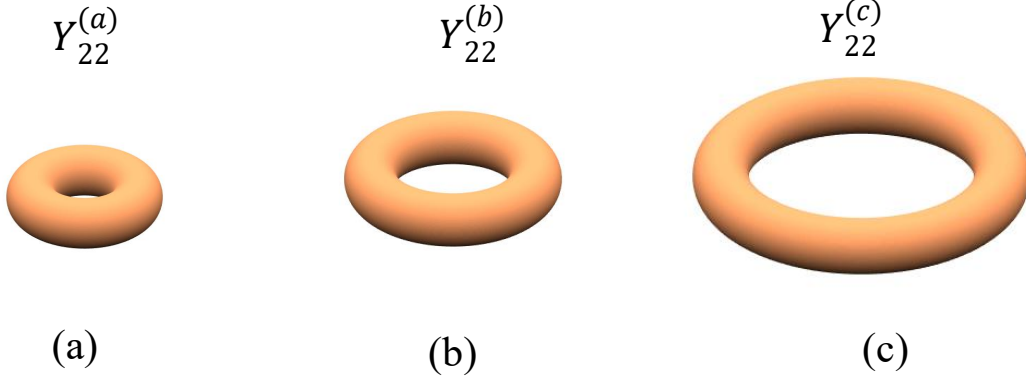


Figure 8: Three conformal nonequivalent tori. The parameters $Y_{22}^{(a)}$, $Y_{22}^{(b)}$, and $Y_{22}^{(c)}$ represent the imaginary part of the modular parameter of the torus (a), (b), and (c), respectively. We have set $Y_{22}^{(c)} > Y_{22}^{(b)} > Y_{22}^{(a)} > 1$. Torus (a) is smaller than torus (b), which in turn is smaller than torus (c).

points $(0, 0)$, $(1, 0)$, $(\text{Re}(\Pi(2)_{22}), \text{Im}(\Pi(2)_{22}))$, $(\text{Re}(\Pi(2)_{22}) + 1, \text{Im}(\Pi(2)_{22}))$, one obtains a parallelogram in the complex plane. The base and height of this parallelogram are 1 and $\text{Im}(\Pi(2)_{22}) = Y_{22}$, respectively. By gluing the parallel edges of this parallelogram together, one obtains a torus [42]. Equation (65) shows that the creation rate $\Gamma(\Pi(2)_{22}, \Pi_{12})$ is independent of the parameter X_{22} . For simplicity, we consider the case where $X_{22} = 0$. In this instance, equation (59) indicates that $Y_{22} \geq 1$. The base of the parallelogram is fixed to 1. Thus, a smaller height Y_{22} corresponds to a smaller torus, as shown in figure 8. Observing figure 8, it can be seen that a torus with a smaller Y_{22} appears “fatter.” When $Y_{12} \neq 0$, this torus connects with the parent universe and becomes a wormhole. Therefore, a smaller Y_{22} corresponds to a smaller wormhole.

Figure 9 illustrates variations in the boundary wormhole creation rate $\Gamma(\Pi(2)_{22}, \Pi_{12})$. Figures 9(a) and 9(c) show that stronger coupling strength corresponds to a larger boundary wormhole creation rate $\Gamma(\Pi(2)_{22}, \Pi_{12})$. Figures 9(a) and 9(b) indicate that as the parameter Y_{22} increases, the boundary wormhole creation rate $\Gamma(\Pi(2)_{22}, \Pi_{12})$ decreases. This suggests that smaller wormholes are easier to create in the parent universe $\lim_{T \rightarrow 0} \text{TAdS}_3$. Figures 9(b) and 9(c) reveal that as the absolute value of the cosmological constant increases, the boundary wormhole creation rate $\Gamma(\Pi(2)_{22}, \Pi_{12})$ also increases. This implies that BWFs are more likely to occur in the AdS_3 spacetime with a more negative cosmological constant. Equation (65) clearly indicates that the boundary wormhole creation rate $\Gamma(\Pi(2)_{22}, \Pi_{12})$ is independent of the integral mea-

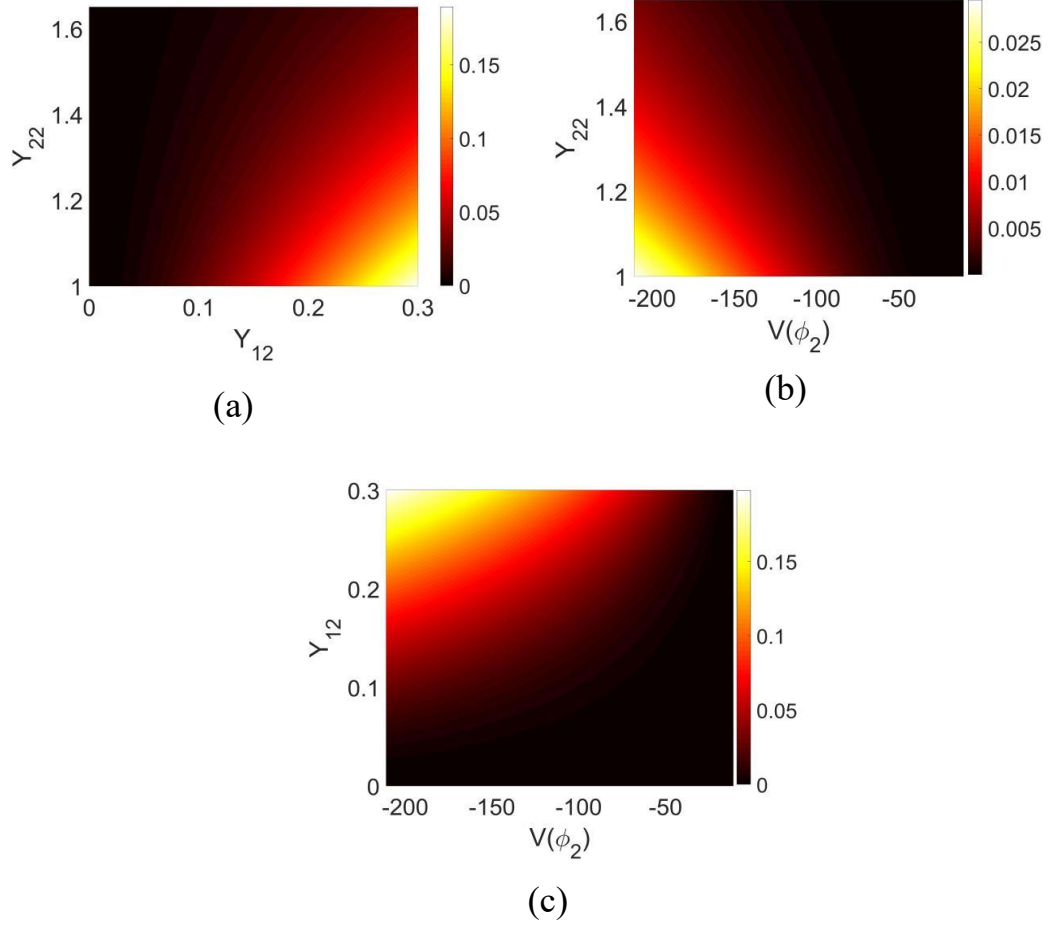


Figure 9: Variations in the boundary wormhole creation rate $\Gamma(\Pi(2)_{22}, \Pi_{12})$. In figures (a) and (b), the vertical axes represent the parameter Y_{22} . In figures (b) and (c), the horizontal axes represent the cosmological constant $V(\phi_2)$. The horizontal axis of figure (a) and the vertical axis of figure (b) represent the coupling strength Y_{12} . Different colors in figures (a), (b) and (c) represent various values of the boundary wormhole creation rate $\Gamma(\Pi(2)_{22}, \Pi_{12})$. The parameters are set as follows: in figure (a), $V(\phi_2) = -200$; in figure (b), $Y_{12} = 0.1$; in figure (c), $Y_{22} = 1$.

sure $d\sigma(g)$. Therefore, the conclusions drawn from figure 9 are also independent of the integral measure.

For multiple BWFs, as shown in figure 2(b), the tunneling rate from the genus zero spacetime state to the genus $g-1$ spacetime state is given by equation (64). Substituting equations (48), (59), and (62) into (64), the tunneling rate $\Gamma(g-1)$ can be written as

$$\begin{aligned} \Gamma(g-1) = & \int_{-\frac{1}{2}}^{\frac{1}{2}} dX_{22} \int_{-\frac{1}{2}}^{\frac{1}{2}} dX_{33} \cdots \int_{-\frac{1}{2}}^{\frac{1}{2}} dX_{gg} \int_{\sqrt{1-X_{22}^2}}^{\infty} dY_{22} \int_{\sqrt{1-X_{33}^2}}^{\infty} dY_{33} \cdots \int_{\sqrt{1-X_{gg}^2}}^{\infty} dY_{gg} \\ & \int_{-\alpha}^{\alpha} dX_{12} \int_{-\alpha}^{\alpha} dX_{13} \cdots \int_{-\alpha}^{\alpha} dX_{1g} \int_0^{\beta} dY_{12} \int_0^{\beta} dY_{13} \cdots \int_0^{\beta} dY_{1g} \\ & \times \prod_{j=2}^g \left(\exp\{-2\pi\Xi(\phi_2)Y_{jj}\} (2\pi Y_{12})^{2\Xi(\phi_2)} (2\pi Y_{1j})^{2\Xi(\phi_2)} \right). \end{aligned} \quad (66)$$

Using the approximation $\sqrt{1-X_{jj}^2} \approx 1 - \frac{1}{2}X_{jj}^2 + o(X_{jj}^4)$, one can complete the integration over the variables $(X_{22}, X_{33}, \dots, X_{gg}, Y_{22}, Y_{33}, \dots, Y_{gg}, X_{12}, X_{13}, \dots, X_{1g}, Y_{12}, Y_{13}, \dots, Y_{1g})$. Consequently, equation (66) simplifies to

$$\Gamma(g-1) = \frac{2\Xi(\phi_2) + 1}{2g\Xi(\phi_2) + 1} \left(\Theta(\phi_2) \operatorname{erfi}\left(\frac{1}{2}\sqrt{\pi\Xi(\phi_2)}\right) \right)^{g-1}, \quad (67)$$

where,

$$\Theta(\phi_2) \equiv 2\alpha \frac{\exp\{-2\pi\Xi(\phi_2)\}}{2\pi\Xi(\phi_2)} \frac{(2\pi)^{4\Xi(\phi_2)}}{2\Xi(\phi_2) + 1} \Xi(\phi_2)^{-\frac{1}{2}} \beta^{4\Xi(\phi_2)+1} \quad (68)$$

and

$$\operatorname{erfi}(x) \equiv \frac{2}{\sqrt{\pi}} \int_0^x e^{t^2} dt = \frac{2}{\sqrt{\pi}} \sum_{k=0}^{\infty} \frac{x^{2k+1}}{(2k+1)k!} \quad (69)$$

is the imaginary error function.

In equation (66), the factor

$$\prod_{j=2}^g \left(\exp\{-2\pi\Xi(\phi_2)Y_{jj}\} (2\pi Y_{12})^{2\Xi(\phi_2)} (2\pi Y_{1j})^{2\Xi(\phi_2)} \right) \quad (70)$$

is equal to $e^{-B_{out}}$. Thus, this factor represents the tunneling probability from the parent universe $\lim_{T \rightarrow 0} \text{TAdS}_3$ to the genus $g-1$ configuration $(\Pi(g)_{22}, \Pi(g)_{33}, \dots, \Pi(g)_{gg}, \Pi(g)_{12}, \Pi(g)_{13}, \dots, \Pi(g)_{1g})$. Up to the leading order of the WKB approximation, it also denotes the tunneling rate.

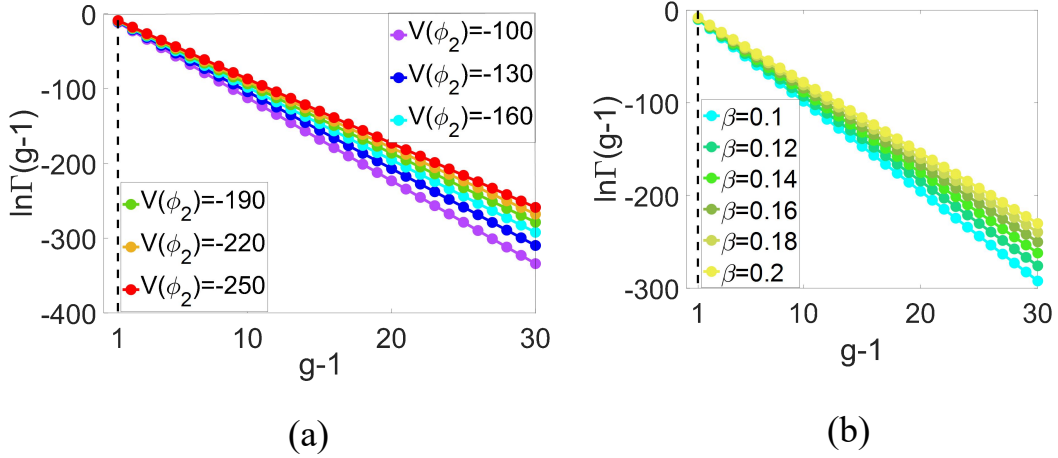


Figure 10: Variations in the tunneling rate $\Gamma(g-1)$ versus genus. In figures (a) and (b), the horizontal axes represent the genus. The vertical axes represent the logarithm of the tunneling rate $\Gamma(g-1)$. The parameters are set as follows: in figure (a), $\alpha = \beta = 0.1$; in figure (b), $\alpha = 0.1$ and $V(\phi_2) = -160$.

Under the dilute wormhole gas approximation, the fluctuations of each wormhole are independent of one another. Thus, the factor (70) can be expressed as the multiplication of the tunneling probabilities of each wormhole. To illustrate this, we temporarily rewrite $e^{-B_{out}}$ in the Schottky space. In the small k_j limit, utilizing equation (34), one can derive

$$e^{-B_{out}} = \prod_{j=2}^g |\sqrt{k_j}(\xi_j - \eta_j)|^{2\Xi(\phi_2)}. \quad (71)$$

It is easy to show that

$$|\sqrt{k_2}(\xi_2 - \eta_2)|^{2\Xi(\phi_2)} = \exp\{-2\pi\Xi(\phi_2)Y_{22}\}(2\pi Y_{12})^{4\Xi(\phi_2)}. \quad (72)$$

Comparing equations (72) and (65), one finds that $|\sqrt{k_2}(\xi_2 - \eta_2)|^{2\Xi(\phi_2)} = \Gamma(\Pi(2)_{22}, \Pi(2)_{12})$. This indicates that the factor $|\sqrt{k_2}(\xi_2 - \eta_2)|^{2\Xi(\phi_2)}$ signifies the tunneling probability of creating the boundary wormhole $(\Pi(2)_{22}, \Pi(2)_{12})$. Therefore, the factor $|\sqrt{k_j}(\xi_j - \eta_j)|^{2\Xi(\phi_2)}$ represents the tunneling probability of creating the boundary wormhole $(\Pi(2)_{jj}, \Pi(2)_{1j})$. Hence, the factor (70) indeed equals the product of the tunneling probabilities of each wormhole.

Figure 10 illustrates the variations in the tunneling rate $\Gamma(g-1)$. Both figures 10(a) and 10(b) show that as the genus increases, the tunneling rate $\Gamma(g-1)$ decreases rapidly, indicating that the dominant fluctuations are those of a single wormhole. This result can also be inferred from another perspective: under the dilute wormhole gas

approximation, the fluctuations of different wormholes are independent of one another. The probability of creating multiple wormholes can be considered as the product of the probabilities of producing each wormhole. Consequently, it becomes more challenging to produce a higher genus spacetime. This leads to a decrease in $\Gamma(g-1)$ with increasing $g-1$. Following this perspective, regardless of the integral measure $d\sigma(g)$ employed, as long as the fluctuations of different wormholes remain independent, one can expect this conclusion to be qualitatively valid.

Figure 10(a) also reveals that in the AdS_3 spacetime with a more negative cosmological constant, the tunneling rate $\Gamma(g-1)$ is larger, which is consistent with the findings from figures 9(b) and 9(c). Figure 10(b) shows that the exact value of the parameter β does not affect the qualitative result. In addition, equations (67) and (68) indicate that $\Gamma(g-1) \propto \alpha^{g-1}$. Therefore, the qualitative results obtained from figure 10 are also unaffected by the specific value of the parameter α .

To sum up, in this section, we demonstrate that the rate of creating the spacetime configuration $(\Pi(2)_{22}, \Pi_{12})$ is described by the quantity $\Gamma(\Pi(2)_{22}, \Pi_{12})$. We show that BWFs are more likely to occur in AdS_3 spacetime with a more negative cosmological constant. We also show that smaller wormholes are easier to create. The total rate of tunneling from the genus zero AdS_3 state to a higher genus spacetime state is described by $\Gamma(g-1)$. The rate $\Gamma(g-1)$ rapidly decreases as the genus increases. Thus, the dominant fluctuations are the genus one fluctuations.

The BWFs break the global spherical symmetry of the universe, as shown in figure 2. Up to now, the existence of wormholes has not been confirmed by experiments. In addition, observations of the cosmic microwave background (CMB) suggest that the observed universe is highly homogeneous and isotropic. In other words, the observed universe approximately exhibits global spherical symmetry. This seems to indicate that the number of large scale wormholes is small (or possibly zero). Thus, a question arises: given that wormholes can be created via quantum tunneling, why is the number of large scale wormholes small? Our calculations for $\Gamma(\Pi(2)_{22}, \Pi_{12})$ and $\Gamma(g-1)$ indicate that macroscopic boundary wormholes are difficult to create, and the probability of creating multiple wormholes is small. These results support the idea that the number of large scale wormholes should indeed be small. Although our calculations are limited to

boundary wormholes in AdS_3 spacetime, we believe that our results provide valuable insights into this question.

5.2 Boundary wormhole fluctuations influence on the false vacuum decay

If wormhole fluctuations are not considered, the vacuum decay rate is given by $e^{-B_{seed}}$. However, when BWFs are taken into account, vacuum decay can occur through multiple pathways. During the decay from the false vacuum state to the true vacuum state, the spacetime may produce various wormholes. All these possible spacetime configurations must be accounted for. Therefore, when considering BWFs, the vacuum decay rate is modified as described in equation (49).

By comparing equations (49) and (64), the relationship between the vacuum decay rate Γ_{tot} and the tunneling rate $\Gamma(g-1)$ is given by

$$\Gamma_{tot} = e^{-B_{seed}} + e^{-B_{seed}} \sum_{g=2}^{\infty} \Gamma(g-1). \quad (73)$$

Substituting equation (67) into (73) yields

$$\Gamma_{tot} = \frac{2\Xi(\phi_2) + 1}{2\Xi(\phi_2)} e^{-B_{seed}} \text{LerchPhi}\left[\Theta(\phi_2) \text{erfi}\left(\frac{1}{2}\sqrt{\pi\Xi(\phi_2)}\right), 1, \frac{2\Xi(\phi_2) + 1}{2\Xi(\phi_2)}\right], \quad (74)$$

where

$$\text{LerchPhi}[x, s, a] \equiv \sum_{n=0}^{\infty} \frac{x^n}{(a+n)^s} \quad (75)$$

is the Lerch transcendent function [68]. In equation (74), the factor $e^{-B_{seed}}$ is the vacuum decay rate predicted by Coleman-De Luccia theory, while the other factors represent the contribution of BWFs.

Figure 11 shows the variations in the vacuum decay rate Γ_{tot} . Figures 11(a) and 11(b) show that as the absolute value of the false vacuum energy density decreases, the vacuum decay rate Γ_{tot} increases. Figure 11(b) indicates that as $|V(\phi_2)|$ decreases, different curves will intersect at one point, implying that the effects of BWFs decrease as $|V(\phi_2)|$ decreases. This result aligns with the result from figures 9(b), 9(c), and figure 10(a). Figure 11(b) also indicates that the vacuum decay rate Γ_{tot} increases with $V(\phi_2)$. In our model, a smaller $V(\phi_2)$ (keeping other parameters fixed) may correspond

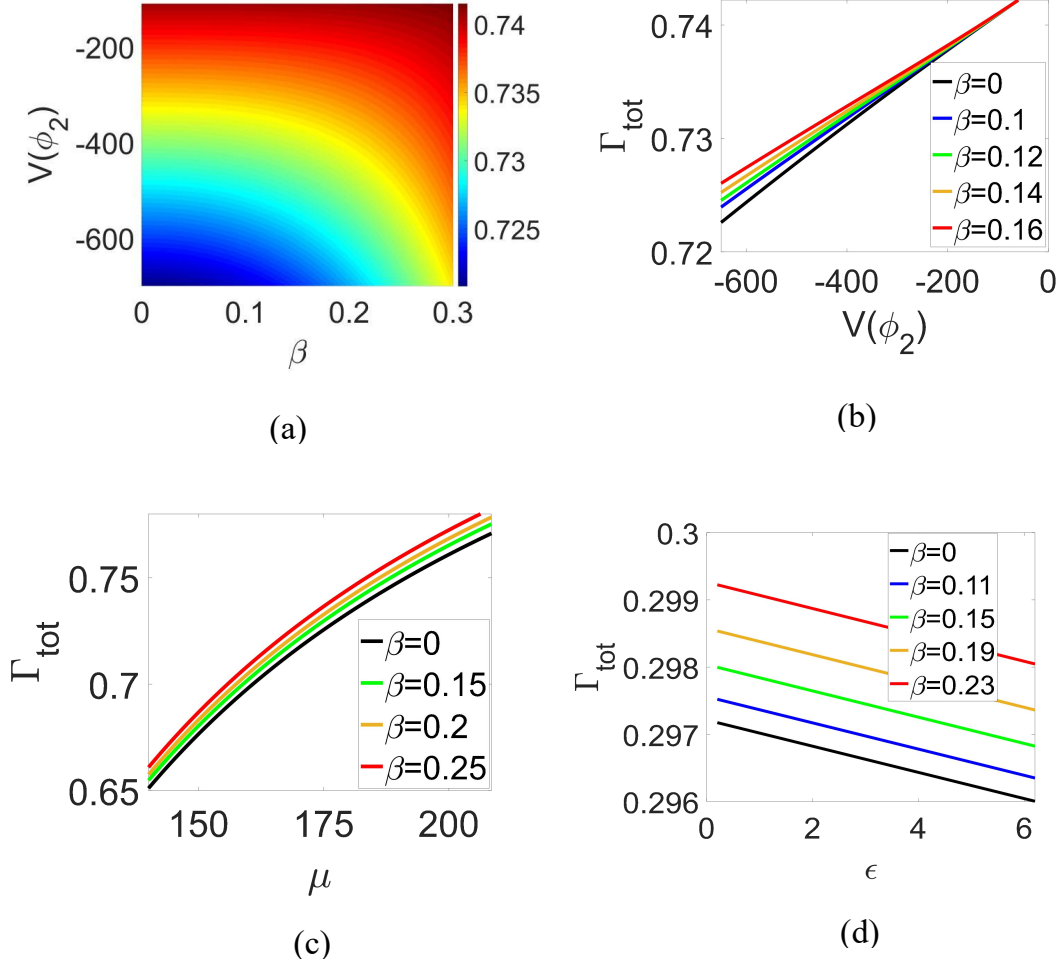


Figure 11: Variations in the vacuum decay rate Γ_{tot} under the condition $\alpha = 0.2$. In figure (a), the horizontal axis and the vertical axis represent the upper limit of the coupling strength Y_{12} and the false vacuum energy density $V(\phi_2)$, respectively. Different colors represent various values of the vacuum decay rate Γ_{tot} . In figures (b), (c) and (d), the vertical axes represent the vacuum decay rate Γ_{tot} . The horizontal axes of figures (b), (c) and (d) represent the false vacuum energy density $V(\phi_2)$, the tension of the domain wall and the difference of the two vacuum energy density, respectively. Different curves correspond to different values of the parameter β . The black curves represent the vacuum decay rate in the Coleman-De Luccia theory. The parameters are set as follows: in figures (a) and (b), $\mu = 150$ and $\epsilon = 0.1$; in figure (c), $V(\phi_2) = -800$ and $\epsilon = 1$; in figure (d), $V(\phi_2) = -500$ and $\mu = 70$.

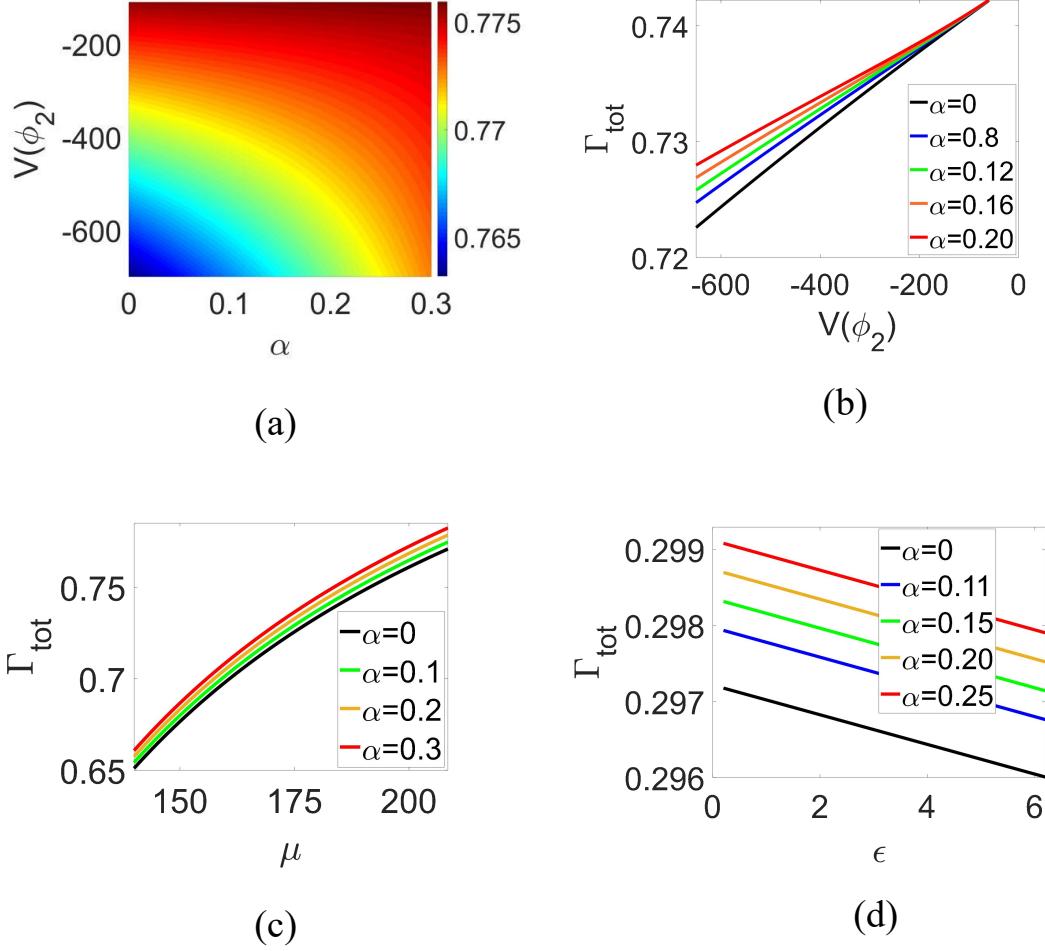


Figure 12: Variations in the vacuum decay rate Γ_{tot} under the condition $\beta = 0.2$. In figure (a), the horizontal axis and the vertical axis represent the upper limit of the coupling strength Y_{12} and the false vacuum energy density $V(\phi_2)$, respectively. Different colors represent different values of the vacuum decay rate Γ_{tot} . In figures (b), (c) and (d), the vertical axes represent the vacuum decay rate Γ_{tot} . The horizontal axes of figures (b), (c) and (d) represent the false vacuum energy density $V(\phi_2)$, the tension of the domain wall and the difference of the two vacuum energy density, respectively. Different curves correspond to different values of the parameter α . The black curves represent the vacuum decay rate in the Coleman-De Luccia theory. The parameters are set as follows: in figure (a), $\mu = 200$ and $\epsilon = 0.1$; in figure (b), $\mu = 170$ and $\epsilon = 0.1$; in figure 12 (c), $V(\phi_2) = -800$ and $\epsilon = 1$; in figure (d), $V(\phi_2) = -500$ and $\mu = 70$.

to a higher potential barrier between the two vacuum states. Thus, figure 11(b) implies that a higher potential barrier corresponds to a harder tunneling. This is a typical feature of quantum tunneling processes. Figure 11(c) reveals that as the tension of the domain wall increases, the vacuum decay rate Γ_{tot} also increases. Furthermore, figure 11(d) shows that a smaller energy density difference between the false vacuum state and the true vacuum state corresponds to a higher vacuum decay rate.

The black curves in figures 11(b), 11(c), and 11(d) represent the variations in the vacuum decay rate without wormhole fluctuations. These figures indicate that including BWFs increases the vacuum decay rate, as more pathways for vacuum decay are considered. This result is valid regardless of the integral measure $d\sigma(g)$. Figures 10(b), 11(a), 11(b), 11(c), and 11(d) illustrate that the specific value of parameter β does not affect the qualitative conclusions. Figure 12 is similar to figure 11, indicating that the particular value of parameter α also has no influence on the qualitative results.

6 Conclusions and discussions

In this work, we studied the BWFs of the AdS_3 spacetime and their influence on false vacuum decay. Our model consists of a real scalar field coupled with the three dimensional general relativity. The scalar potential has two minimal values, corresponding to two vacuum states. According to Coleman-De Luccia theory, the vacuum decay rate is determined by the total tunneling action, which consists of the Euclidean action of the bounce solution and a background term. Under the thin wall approximation, the bounce solution can be visualized as a spherically symmetric bubble embedded in a sea of false vacuum. The total tunneling action can be divided into three components: the tunneling action inside, within, and outside the domain wall. For convenience, we define the vacuum decay seed as the sum of the tunneling action inside and on the domain wall. Without wormhole fluctuations, the tunneling action outside the bubble is zero, making the total tunneling action equivalent to the vacuum decay seed.

We demonstrate that in the presence of BWFs, the tunneling action outside the bubble becomes nonzero. The volume of AdS_3 spacetime is infinite. Thus, studying the tunneling action outside the bubble requires regularizing the volume and action of spacetime. Both the regularized action and the original Einstein-Hilbert action

correspond to the same spacetime dynamical equations.

We categorize wormhole fluctuations into three classes. In the first class, both ends of the wormhole is inside the bubble. In the second class, one end of the wormhole is inside the bubble while the other is outside. In the third class, both ends of the wormhole are outside the bubble. Fluctuations of the third class do not affect the vacuum decay seed. Our focus is on the scenario where the bubble radius is much smaller than the size of AdS_3 spacetime. In this case, the third class of fluctuations is predominant. Thus, we disregard the first and second classes of fluctuations.

The three dimensional high genus spacetime includes handlebodies and non-handlebodies. Some researchers argue that the effects of the handlebodies are predominant. Thus, for simplicity, we focus on the contributions of the handlebodies. All three dimensional handlebodies can be obtained by filling the interior of a closed high genus Riemann surface. Therefore, summing over different handlebodies is equivalent to summing over various closed Riemann surfaces. There are different methods to classify the closed Riemann surfaces. Both Schottky space and the Siegel upper half space can be used to parameterize different closed Riemann surfaces. The summation over different closed Riemann surfaces translates into an integration in these two spaces.

The regularized action of the high genus AdS_3 spacetime in Schottky space is helpful in deriving the tunneling action of the high genus spacetime. Thus, at first, we formulate the tunneling action in Schottky space. However, it is easier to define the integral domain in the Siegel upper half space. Therefore, we transform the tunneling action from Schottky space into the Siegel upper half space. This transformation can be simplified using the dilute wormhole gas approximation.

In the Siegel upper half space, various handlebodies are characterized by different period matrices. The off-diagonal elements are interpreted as the interactions between different wormholes or between the parent universe and the wormholes. Under the dilute wormhole gas approximation, the interactions between different wormholes are small. However, this does not imply that the interactions between the parent universe and the wormholes are also necessarily small. To simplify the tunneling action, we assume that the interactions among different wormholes are significantly smaller compared to the interactions between the parent universe and the wormholes.

Different handlebodies can be interpreted as various BWFs. We show that BWFs are more likely to occur in AdS_3 spacetime with a more negative cosmological constant. We find that smaller wormholes are easier to create. The summation over different BWFs involves integration in the Siegel upper half space. We demonstrate that the integral domain is a subspace of the fundamental domain of the modular group $\text{Sp}(2g, \mathbb{Z})$ in the Siegel upper half space. Upon completing the integration, we obtain the tunneling rate from the genus zero spacetime state to the high genus spacetime state. We find that as the genus increases, the tunneling rate decreases rapidly. Thus, the primary fluctuations are the genus one fluctuations. Taking into account the BWFs, the vacuum decay rate will increase. In our model, despite there being two unfixed parameters, we have demonstrated that the specific values of these parameters do not affect any qualitative results.

Acknowledgements

Hong Wang was supported by the National Natural Science Foundation of China Grant No. 21721003. No.12234019. Hong Wang thanks for the help from Professor Erkang Wang.

A Schottky parametrization of the AdS_3 handlebody

The parameterization of the AdS_3 handlebody is essential for studying BWFs. Under a specific cosmological constant, the distinctions between various AdS_3 handlebodies are determined by their conformal boundaries. Thus, to parameterize an AdS_3 handlebody, it suffices to parameterize its conformal boundary. The conformal boundary of any AdS_3 handlebody is a two dimensional closed Riemann surface. There are several methods for parameterizing the two dimensional closed Riemann surface. Different parameterization methods may correspond to different ways of constructing the closed Riemann surface. We focus on the Schottky parameterization. The mathematics reviewed in this section can be found in references [52, 69].

The Schottky group is a discrete subgroup of the two dimensional special complex

linear transformation group $SL(2, \mathbb{C})$. The elements of the Schottky group can be expressed as

$$\mathcal{T} = \begin{pmatrix} a & b \\ c & d \end{pmatrix}, \quad (76)$$

where a, b, c and d are complex numbers satisfying $ad - bc = 1$. The Riemann sphere \mathbb{S} is a two dimensional complex sphere. The operation of the Schottky group on the Riemann sphere can be written as

$$\mathcal{T}(z) = \frac{az + b}{cz + d}. \quad (77)$$

Here, “ z ” represents a point on the Riemann sphere. We use the symbol $\mathbf{Sch}(L_1, L_2, \dots, L_g)$ to represent the genus g Schottky group, where L_1, L_2, \dots, L_g represent its generators. $\mathbf{Sch}(L_1, L_2, \dots, L_g)$ is freely generated by L_1, L_2, \dots, L_g . That is, any element of $\mathbf{Sch}(L_1, L_2, \dots, L_g)$ can be written in the form $L_{r_1}^{n_1} L_{r_2}^{n_2} \dots L_{r_m}^{n_m}$, where $r_i = 1, 2, \dots, g$ and $n_i = \pm 1, \pm 2, \dots$.

Any genus g closed Riemann surface can be constructed by the operation of the genus g Schottky group on the Riemann sphere [11, 20, 52, 70]. The operation of a generator L_i of the genus g Schottky group on the Riemann sphere can always be expressed as [11, 52, 70]

$$\frac{L_i(z) - \xi_i}{L_i(z) - \eta_i} = k_i \frac{z - \xi_i}{z - \eta_i}. \quad (78)$$

Here, $i = 1, 2, \dots, g$. ξ_i and η_i are the attractive and the repelling fixed point of the generator L_i , respectively, and k_i is the multiplier with $|k_i| < 1$. For a normalized Schottky group, $\xi_1 = 0$, $\xi_2 = 1$, and $\eta_1 = \infty$. For a marked Schottky group, the generators L_1, L_2, \dots, L_g are ordered. Both normalized and marked conditions are necessary to parameterize the two dimensional closed Riemann surface. Henceforth, when referring to the Schottky group, we assume it is both normalized and marked.

Equation (78) indicates that $L_i(z)$ can be written as

$$L_i(z) = \frac{\eta_i(z - \xi_i) - k_i \xi_i(z - \eta_i)}{(z - \xi_i) - k_i(z - \eta_i)}. \quad (79)$$

By comparing equations (76), (77), and (79), one can read off the matrix representation of the generator L_i as

$$L_i = \frac{1}{\sqrt{|k_i|}|\eta_i - \xi_i|} \begin{pmatrix} \xi_i - k_i \eta_i & -\eta_i \xi_i(1 - k_i) \\ 1 - k_i & k_i \xi_i - \eta_i \end{pmatrix}. \quad (80)$$

According to equation (80), one can obtain the matrix representation of any element in the Schottky group $\mathbf{Sch}(L_1, L_2, \dots, L_g)$.

Denoting the multiplier of the element $L_i L_j$ as k_{ij} , the relationship between k_{ij} and the parameters $(\xi_i, \eta_i, k_i, \xi_j, \eta_j, k_j)$ is given by [52]

$$k_{ij} = \frac{\det(L_i L_j)}{(\text{Tr}(L_i L_j))^2} + o(k_i^2, k_j^2) \approx k_i k_j \frac{(\eta_i - \xi_i)^2 (\eta_j - \xi_j)^2}{(\eta_j - \xi_i)^2 (\eta_i - \xi_j)^2}. \quad (81)$$

Here, $\det(L_i L_j)$ and $\text{Tr}(L_i L_j)$ represent the determinant and the trace of the element $L_i L_j$, respectively, and $o(k_i^2, k_j^2)$ represents higher order terms of the multipliers k_i and k_j . It is worth noting that $L_i(z)$ and $L_i^{-1}(z)$ share the same multiplier. Thus, according to equation (81), one can prove that the multipliers of the elements $L_i L_j$, $L_j L_i$, $L_i^{-1} L_j^{-1}$, and $L_j^{-1} L_i^{-1}$ are equivalent. Similarly, the multipliers of the elements $L_i^{-1} L_j$, $L_i L_j^{-1}$, $L_j^{-1} L_i$, and $L_j L_i^{-1}$ are also equivalent [52]. Therefore, up to the first order of the multipliers, the Schottky group $\mathbf{Sch}(L_1, L_2, \dots, L_g)$ can be approximated as

$$\mathbf{Sch}(L_1, L_2, \dots, L_g) \approx \{id, L_i, L_i^{-1} \mid i = 1, 2, \dots, g\}. \quad (82)$$

Here, id represents the identity element of the Schottky group. The second order approximation is

$$\begin{aligned} \mathbf{Sch}(L_1, L_2, \dots, L_g) \approx \{ & id, L_i, L_i^{-1}, L_i L_j, L_i L_j^{-1}, L_i^{-1} L_j, L_i^{-1} L_j^{-1}, \\ & L_i^2, (L_i^{-1})^2 \mid i, j = 1, 2, \dots, g; i \neq j\}. \end{aligned} \quad (83)$$

Equation (78) indicates that L_i is determined by the parameters ξ_i, η_i , and k_i . The genus g Schottky group $\mathbf{Sch}(L_1, L_2, \dots, L_g)$ is determined by its generators L_1, L_2, \dots, L_g . In addition, the normalized conditions of the Schottky group are $\xi_1 = 0, \xi_2 = 1$ and $\eta_1 = \infty$. Thus, a genus g Schottky group is determined by the set of parameters $(k_1, \eta_2, k_2, \xi_3, \eta_3, k_3, \dots, \xi_g, \eta_g, k_g)$. For a genus one Schottky group $\mathbf{Sch}(L_1)$, there is only one generator L_1 . Thus, it is determined by the parameters ξ_1, η_1, k_1 . However, ξ_1, η_1 are fixed by the normalized conditions. Therefore, the genus one Schottky group is completely determined by the multiplier k_1 .

Different sets of parameters $(k_1, \eta_2, k_2, \xi_3, \eta_3, k_3, \dots, \xi_g, \eta_g, k_g)$ correspond to various Schottky groups. All genus g ($g \geq 2$) Schottky groups form the genus g Schottky space. For genus $g \geq 2$, the vector $(k_1, \eta_2, k_2, \xi_3, \eta_3, k_3, \dots, \xi_g, \eta_g, k_g)$ represents a point in the space \mathbb{C}^{3g-3} (\mathbb{C} is the complex plane). Thus, the dimension of the genus g ($g \geq 2$)

Schottky space is $6g - 6$. Similarly, the dimension of the genus one Schottky space is two. Therefore, the dimension of the genus g Schottky space equals the dimension of the genus g Teichmüller space, which consists of the conformal equivalence classes of marked genus g Riemann surfaces. Furthermore, the Teichmüller space is the universal cover of the Schottky space.

We use Σ_g to denote the genus g closed Riemann surface. Then Σ_g can be constructed by the operation of the Schottky group on the Riemann sphere \mathbb{S} [20]:

$$\Sigma_g = (\mathbb{S} - \mathbf{Fix}) / \mathbf{Sch}(L_1, L_2, \dots, L_g). \quad (84)$$

Here, \mathbf{Fix} denotes the set of fixed points of the Schottky group. A fixed point of an element L in the Schottky group is a point $z_0 \in \mathbb{S}$ that satisfies $L(z_0) = z_0$. The term $\mathbb{S} - \mathbf{Fix}$ represents the deletion of the fixed points from the Riemann sphere \mathbb{S} . Equation (84) represents the Schottky parameterization of the Riemann surface Σ_g . The Schottky parameterization of Σ_g models Σ_g as the quotient of $(\mathbb{S} - \mathbf{Fix})$ by the Schottky group $\mathbf{Sch}(L_1, L_2, \dots, L_g)$.

Equation (84) can be roughly interpreted in an intuitive way [20]. On the Riemann sphere \mathbb{S} , one can choose $2g$ non-intersecting circles $C_1, C'_1, C_2, C'_2, \dots, C_g, C'_g$ such that each circle lies entirely outside the others. These circles are known as the Schottky circles. Cut out the interior of each circle. Finally, glue each pair of circles C_i and C'_i together to form a closed surface. The resulting surface is the Riemann surface Σ_g .

Equation (84) shows that a Schottky group corresponds to a Riemann surface Σ_g . Thus, every point in the Schottky space corresponds to a Riemann surface Σ_g . Therefore, the sets of parameters $(k_1, \eta_2, k_2, \xi_3, \eta_3, k_3, \dots, \xi_g, \eta_g, k_g)$ can be used to distinguish different Riemann surfaces Σ_g . The AdS_3 handlebody can be obtained by “filling” the interior of the Riemann surface Σ_g . Therefore, the Schottky space can describe various AdS_3 handlebodies.

The Schottky space is useful for representing the regularized action of the AdS_3 handlebody. However, it is less convenient for summing over physically non-equivalent AdS_3 handlebody spacetimes. This limitation arises because different points in the Schottky space may correspond to the same Riemann surface, and the Schottky space is not simply connected [20]. In our model, the Siegel upper half space ($\mathbf{Sie}(g)$) offers a more convenient framework for summing over different AdS_3 handlebodies.

B Relationship between the period matrix and the Schottky group

The period matrix can also be used to distinguish between different Riemann surfaces Σ_g . It belongs to the elements of the space $\mathbf{Sie}(g)$. The relationship between the period matrix and the Schottky group facilitates the transformation of functions from the Schottky space to the space $\mathbf{Sie}(g)$. The space $\mathbf{Sie}(g)$ is convenient for defining the integral domain when summing over different AdS_3 handlebodies.

The generators of the homology group of the Riemann surface Σ_g are denoted as $\{A^1, A^2, \dots, A^g; B_1, B_2, \dots, B_g\}$. All of them are non-contractible circles on Σ_g . Figure 13 depicts the relationship between the circles A^i , B_i and C_i , C'_i . A similar figure can be found in references [52, 71]. The period matrix is defined as [56, 72]

$$\Pi(g)_{ij} \equiv \oint_{B_j} \omega_i, \quad (85)$$

where ω_i is defined by [52, 69]

$$\omega_i \equiv \sum_{\mathcal{T} \in \mathbf{Sch}|L_i} \left(\frac{1}{z - \mathcal{T}(\eta_i)} - \frac{1}{z - \mathcal{T}(\xi_i)} \right) dz. \quad (86)$$

Here, the summation $\sum_{\mathcal{T} \in \mathbf{Sch}|L_i}$ is over all elements \mathcal{T} of the Schottky group $\mathbf{Sch}(L_1, L_2, \dots, L_g)$, excluding those with L_i^n ($n = \pm 1, \pm 2, \dots$) as their rightmost factor. ω_i is a holomorphic differential on the Riemann surface Σ_g . It is normalized along the A^i circle, that is, $\oint_{A^i} \omega_i = 2\pi i \delta_{ij}$.

Substituting equation (86) into (85), and completing the integration along the B_j circle, one obtains [52, 69, 73]

$$2\pi i \Pi(g)_{ij} = \delta_{ij} \ln(k_i) + \sum_{\mathcal{T} \in L_i | \mathbf{Sch}|L_j} \ln \left(\frac{(\eta_i - \mathcal{T}(\eta_j))(\xi_i - \mathcal{T}(\xi_j))}{(\eta_i - \mathcal{T}(\xi_j))(\xi_i - \mathcal{T}(\eta_j))} \right), \quad (87)$$

where the summation $\sum_{\mathcal{T} \in L_i | \mathbf{Sch}|L_j}$ is over all elements \mathcal{T} of the Schottky group $\mathbf{Sch}(L_1, L_2, \dots, L_g)$, excluding those with L_i^n ($n = \pm 1, \pm 2, \dots$) as the leftmost factor or L_j^n as the rightmost factor. In the case where $i = j$, the identity element of $\mathbf{Sch}(L_1, L_2, \dots, L_g)$ is also excluded from the summation.

Equation (87) establishes the relationship between the period matrix and the Schottky group. However, it is difficult to calculate the summation on the right hand side

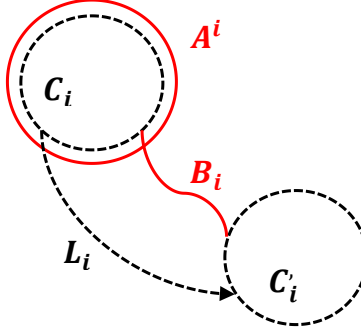


Figure 13: Diagram of the Schottky circles and the canonical homology bases of circles. The black dashed circles represent the Schottky circles, while the red curves represent the canonical homology bases of circles. This figure is drawn on the Riemann sphere. The two ends of the curve B_i become the same point after the operation of the Schottky group.

of equation (87) strictly. A first order approximation (82) of the Schottky group $\mathbf{Sch}(L_1, L_2, \dots, L_g)$ suffices for our model (see appendix A). Under this approximation, only the elements $\{L_j, L_j^{-1} \mid j = 1, 2, \dots, g; j \neq i\}$ contribute to the summation in equation (87) when calculating the element $\Pi(g)_{ii}$. For the calculation of the non-diagonal element $\Pi(g)_{ij}$ ($i \neq j$), one only needs to sum over the elements $\{id, L_n, L_n^{-1} \mid n = 1, 2, \dots, g; n \neq i; n \neq j\}$.

Using this approximation, the period matrix can be simplified to

$$2\pi i \Pi(g)_{ii} = \ln(k_i) + \sum_{n \neq i} \frac{2k_n(\xi_i - \eta_i)^2(\xi_n - \eta_n)^2}{(\xi_i - \xi_n)(\eta_i - \eta_n)(\eta_i - \xi_n)(\xi_i - \eta_n)} + \sum_{n \neq i} o(k_n^2), \quad (88)$$

$$2\pi i \Pi(g)_{ij} = \ln \frac{(\eta_i - \eta_j)(\xi_i - \xi_j)}{(\eta_i - \xi_j)(\xi_i - \eta_j)} + \sum_{n \neq i, j} \frac{2k_n(\xi_n - \eta_n)^2(\eta_i - \xi_i)(\eta_j - \xi_j)}{(\eta_i - \xi_n)(\xi_i - \xi_n)(\eta_j - \eta_n)(\xi_j - \eta_n)} + \sum_{n \neq i, j} o(k_n^2). \quad (89)$$

In equation (88), $n = 1, 2, \dots, g$ and $n \neq i$. In equation (89), $n = 1, 2, \dots, g$ and $n \neq i, j$. To derive equations (88) and (89) from (87), we used the formula [52]

$$\frac{(z_1 - L_i(\sigma_1))(z_2 - L_i(\sigma_2))}{(z_1 - L_i(\sigma_2))(z_2 - L_i(\sigma_1))} = 1 + \frac{k_i(\xi_i - \eta_i)^2(z_1 - z_2)(\sigma_1 - \sigma_2)}{(z_1 - \xi_i)(z_2 - \xi_i)(\sigma_1 - \eta_i)(\sigma_2 - \eta_i)} + o(k_i^2). \quad (90)$$

Here, $z_1, z_2, \sigma_1, \sigma_2$ are points on the Riemann surface Σ_g . In the case where the Schottky group contains only two generators, equations (88) and (89) reduce to equation (A.28) in reference [52].

Different AdS_3 handlebody spacetimes can be characterized by the period matrix. For instance, the conformal boundary of the Euclidean thermal AdS_3 spacetime (TAdS_3)

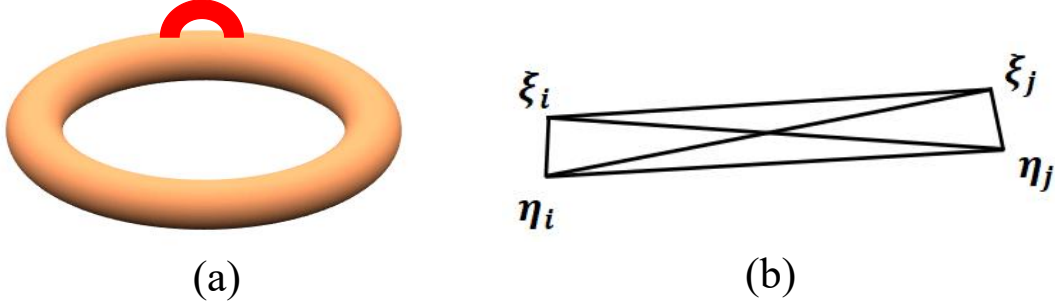


Figure 14: A diagram illustrating boundary wormhole fluctuations and the dilute wormhole gas approximation. Figure (a) depicts the boundary wormhole fluctuations, while figure (b) illustrates the dilute wormhole gas approximation. In figure (a), the orange torus represents the conformal boundary of a Euclidean thermal AdS_3 spacetime, and the red strip represents a wormhole with two ends. In figure (b), ξ_i and η_i approximately denote the two ends of one wormhole, while ξ_j and η_j represent the two ends of another wormhole.

is a torus. The period matrix of a torus is a complex number, which is the modular parameter of the torus. The real part of the period matrix for TAdS_3 corresponds to the angular potential, while its imaginary part corresponds to the inverse of temperature. The time circle in TAdS_3 is non-contractible. Figure 14(a) illustrates the creation of a wormhole in TAdS_3 . The resulting spacetime is a genus two handlebody, where the period matrix is a 2×2 symmetric matrix.

Equations (88) and (89) are still complicated. We need to simplify them further. To achieve this, we consider the dilute wormhole gas approximation [53, 55], which implies that the size of the wormholes is much smaller than their distance. Note that under the small k_i limit, ξ_i and η_i approximately represent the two ends of the wormhole [53]. Thus, in this case, one can use the equation

$$|\xi_i - \eta_i| \ll |\xi_i - \eta_j| \quad (i \neq j) \quad (91)$$

to represent the dilute wormhole gas approximation. Figure 14(b) depicts the dilute wormhole gas approximation visually. It also illustrates that the differences between $|\xi_i - \eta_j|$, $|\xi_i - \xi_j|$, and $|\eta_i - \eta_j|$ ($i \neq j$) are small.

Using equation (91), the period matrix in equations (88) and (89) can be approximated as

$$2\pi i \Pi(g)_{ii} \approx \ln(k_i), \quad (92)$$

$$2\pi i \Pi(g)_{ij} \approx \ln \frac{(\eta_i - \eta_j)(\xi_i - \xi_j)}{(\eta_i - \xi_j)(\xi_i - \eta_j)}. \quad (93)$$

Equations (92) and (93) describe the relationship between the period matrix and the Schottky group under the dilute wormhole gas approximation. These two equations are consistent with formula (3.3) in reference [53]. In addition, when deriving equations (92) and (93), we have used the small k_j limit. In this limit, $1 - \exp(2\pi i \Pi(g)_{jj}) \approx 1$ (this approximation had been used by Lyons and Hawking in [53]).

Following the discussions by Lyons and Hawking in reference [53], if the generators L_i and L_j correspond to different wormholes, the element $\Pi(g)_{ij}$ ($i \neq j$) can be interpreted as the interaction between wormholes i and j . Thus, equation (93) indicates that the interactions between different wormholes are small under the dilute wormhole gas approximation. In a special case where all non-diagonal elements of the period matrix are zero, $\Pi(g) = \Pi(g)_{11} \oplus \Pi(g)_{22} \oplus \cdots \oplus \Pi(g)_{gg}$, representing a set of disconnected tori, with the modular parameter of the i -th torus being $\Pi(g)_{ii}$.

The Siegel upper half space $\mathbf{Sie}(g)$ consists of all $g \times g$ symmetric matrices where the imaginary part of each matrix element is positive [57]. Formally, the space $\mathbf{Sie}(g)$ is defined as $\mathbf{Sie}(g) \equiv \{\Omega \mid \Omega_{ij} = \Omega_{ji}, \text{Im}(\Omega_{ij}) > 0\}$. The $g \times g$ period matrix is also symmetric ($\Pi(g)_{ij} = \Pi(g)_{ji}$) and belongs to the elements of the space $\mathbf{Sie}(g)$. Equations (92) and (93) facilitate transforming the tunneling action from the Schottky space to the space $\mathbf{Sie}(g)$. This helps in summing over different AdS_3 handlebodies.

C Derivation for the vacuum decay seed B_{seed}

In the region $\rho < \rho_s$, it can be shown that equation (11) reduces to

$$S_E(\rho \leq \rho_s) = 8\pi \int_0^{\rho_s} d\tau_E \{ -1 + \rho^2 V(\phi) \}. \quad (94)$$

Inside the bubble, $\phi_{bounce} = \phi_1$, $\dot{\phi} = 0$ and $d\rho = \sqrt{1 - \rho^2 V(\phi_1)} d\tau_E$. This relationship can be derived from equation (10) by setting $\dot{\phi} = 0$. Combining equations (4) and (94) with these conclusions, the tunneling action B_{in} becomes

$$B_{in} = -8\pi \int_0^{\bar{\rho}} d\rho [1 - \rho^2 V(\phi_1)]^{\frac{1}{2}} + 8\pi \int_0^{\bar{\rho}} d\rho [1 - \rho^2 V(\phi_2)]^{\frac{1}{2}}. \quad (95)$$

Using the integral formula

$$\int_0^a \sqrt{1 - bx^2} dx = \frac{1}{2} \{ a\sqrt{1 - a^2 b} + b^{-\frac{1}{2}} \arcsin(a\sqrt{b}) \}, \quad (96)$$

and performing the integral over the variable ρ , then equation (95) becomes

$$B_{in} = 4\pi \left\{ V^{-\frac{1}{2}}(\phi_2) \arcsin(\bar{\rho}\sqrt{V(\phi_2)}) - V^{-\frac{1}{2}}(\phi_1) \arcsin(\bar{\rho}\sqrt{V(\phi_1)}) \right\} \\ + 4\pi\bar{\rho} \left\{ \sqrt{1 - \bar{\rho}^2 V(\phi_2)} - \sqrt{1 - \bar{\rho}^2 V(\phi_1)} \right\}. \quad (97)$$

Equation (97) represents the tunneling action inside the bubble.

The tension (μ) of the domain wall is given by $\mu = \int_{\phi_1}^{\phi_2} d\phi \sqrt{2(V(\phi) - V(\phi_2))}$. Under the thin wall approximation, the tension μ and the tunneling action B_{wall} are equal to the energy density and the total energy of the domain wall, respectively [74]. Therefore, the tunneling action B_{wall} is

$$B_{wall} = 4\pi\bar{\rho}^2\mu = 4\pi\bar{\rho}^2 \int_{\phi_1}^{\phi_2} d\phi \sqrt{2(V(\phi) - V(\phi_2))}. \quad (98)$$

Equation (98) is the lower dimensional version of equation (2.15) in reference [40]. A more detailed explanation of this method for calculating the tunneling action can be found in [40].

From equations (14), (97) and (98), the vacuum decay seed B_{seed} can be expressed as

$$B_{seed} = 4\pi \left\{ V^{-\frac{1}{2}}(\phi_2) \arcsin(\bar{\rho}\sqrt{V(\phi_2)}) - V^{-\frac{1}{2}}(\phi_1) \arcsin(\bar{\rho}\sqrt{V(\phi_1)}) \right. \\ \left. + \bar{\rho}\sqrt{1 - \bar{\rho}^2 V(\phi_2)} - \bar{\rho}\sqrt{1 - \bar{\rho}^2 V(\phi_1)} + \bar{\rho}^2\mu \right\}. \quad (99)$$

By taking $\partial B/\partial\bar{\rho} = 0$, the bubble radius $\bar{\rho}$ can be obtained as

$$\bar{\rho} = \frac{2\mu}{\sqrt{\mu^4 + \epsilon^2 + 2\mu^2(2V(\phi_2) + \epsilon)}}. \quad (100)$$

Equation (100) indicates that the radius $\bar{\rho}$ is determined by the tension of the domain wall and the energy density of the vacuum states.

D Derivation for equation (46)

The tunneling action B_{out} in equation (44) is complicated, so we need to simplify it. Defining $\mathcal{E}_j \equiv \xi_j - \eta_j$, then equation (93) implies that the element $\Pi(g)_{2j}$ can be expressed as

$$\Pi(g)_{2j} = \frac{1}{2\pi i} \ln \left(1 + \frac{\mathcal{E}_j}{\eta_2 - \xi_j} + \frac{\mathcal{E}_j}{\eta_j - \xi_2} - \frac{\mathcal{E}_j^2}{(\eta_2 - \xi_j)(\xi_2 - \eta_j)} \right). \quad (101)$$

Under the dilute wormhole gas approximation, where the size of the wormholes is significantly smaller than the distance between them (equation (91)). Thus, equation (101) can be approximated as

$$\Pi(g)_{2j} \approx \frac{1}{2\pi i} \left(\frac{\mathcal{E}_j}{\eta_2 - \xi_j} + \frac{\mathcal{E}_j}{\eta_j - \xi_2} \right). \quad (102)$$

Equation (102) indicates that under the dilute wormhole gas approximation, the element $\Pi(g)_{2j}$ is small.

However, the element $\Pi(g)_{1j}$ represents the interaction between the parent universe and the wormhole. The dilute wormhole gas approximation does not imply that $\Pi(g)_{1j}$ is small. Therefore, from equations (41)-(43), the quantities Δ_{1j} , Δ_{2j} , and Δ_{3j} can be approximated as:

$$\Delta_{1j} \approx 1 - \exp(2\pi i \Pi(g)_{1j}), \quad \Delta_{3j} \approx 0, \quad (103)$$

$$\Delta_{2j} \approx (1 - \exp(2\pi i \Pi(g)_{1j})) (1 - \exp(-2\pi i \Pi(g)_{12})). \quad (104)$$

Equations (103) and (104) imply that the interactions between different wormholes are neglected, while the interactions between the parent universe and the wormholes are retained.

Substituting equations (103) and (104) into equation (44), one obtains $B_{out} = \infty$ or

$$B_{out} = \frac{-4\pi}{\sqrt{-V(\phi_2)}} \left\{ \sum_{j=2}^g \ln \left| \frac{\exp(\pi i \Pi(g)_{jj}) (\exp(2\pi i \Pi(g)_{1j}) - 1)}{1 - \exp(2\pi i \Pi(g)_{jj})} \right| + \sum_{j=2}^g \ln \left| (\exp(-2\pi i \Pi(g)_{12}) - 1) \right| \right\}. \quad (105)$$

The symbol “ \pm ” in equation (44) corresponds to two different tunneling actions B_{out} . The case $B_{out} = \infty$ (associated with “ $+$ ”) is unphysical and is therefore disregarded. Equation (105) corresponds to the “ $-$ ” case.

The period matrix can be written as $\Pi(g) = X + iY$. Then, it is straightforward to

prove that

$$\begin{aligned}
& \left| \frac{\exp(\pi i \Pi(g)_{jj})(\exp(2\pi i \Pi(g)_{1j}) - 1)}{1 - \exp(2\pi i \Pi(g)_{jj})} (\exp(-2\pi i \Pi(g)_{12}) - 1) \right| \\
&= \exp(-\pi Y_{jj}) \cdot \left(\exp(-4\pi Y_{jj}) - 2\cos(2\pi X_{jj})\exp(-2\pi Y_{jj}) + 1 \right)^{-\frac{1}{2}} \\
&\quad \times \left(\exp(-4\pi Y_{1j}) - 2\cos(2\pi X_{1j})\exp(-2\pi Y_{1j}) + 1 \right)^{\frac{1}{2}} \\
&\quad \times \left(\exp(4\pi Y_{12}) - 2\cos(2\pi X_{12})\exp(2\pi Y_{12}) + 1 \right)^{\frac{1}{2}}.
\end{aligned} \tag{106}$$

Combining equations (45), (105) and (106), the tunneling action B_{out} can be expressed as

$$\begin{aligned}
B_{out} = & -\Xi(\phi_2)(g-1)\ln\left(1 + \exp(4\pi Y_{12}) - 2\cos(2\pi X_{12})\exp(2\pi Y_{12})\right) \\
& -\Xi(\phi_2)\sum_{j=2}^g \left\{ -2\pi Y_{jj} - \ln\left(1 + \exp(-4\pi Y_{jj}) - 2\cos(2\pi X_{jj})\exp(-2\pi Y_{jj})\right) \right. \\
& \left. + \ln\left(1 + \exp(-4\pi Y_{1j}) - 2\cos(2\pi X_{1j})\exp(-2\pi Y_{1j})\right) \right\}.
\end{aligned} \tag{107}$$

References

- [1] M. Lachièze-Rey and J. P. Luminet, Cosmic topology, Phys. Rep. **254** (1994) 135.
- [2] E. Witten, Topology changing amplitudes in (2+1)-dimensional gravity, Nucl. Phys. B **323** (1989) 113.
- [3] D. Birmingham, M. Blau, M. Rakowski and G. Thompson, Topological Field Theory, Phys. Rep. **209** (1991) 129.
- [4] S. W. Hawking, Wormholes in spacetime, Phys. Rev. D **37** (1988) 904.
- [5] A. Anderson and B. S. DeWitt, Does the topology of space fluctuate?, Found. Phys. **16** (1986) 91.
- [6] S. Carlip and R. Cosgrove, Topology change in (2+1)-dimensional gravity, J. Math. Phys. **35** (1994) 5477.
- [7] S. Carlip and S. P. De Alwis, Wormholes in 2+1 dimension, Nucl. Phys. B **337** (1990) 681.

- [8] B. Bahr, On background-independent renormalization of spin foam models, *Class. Quant. Grav.* **34** (2017) 075001.
- [9] E. Witten, (2+1)-Dimensional gravity as an exactly soluble system, *Nucl. Phys. B* **311** (1988) 46.
- [10] S. Carlip, Spacetime foam: a review, *Rept. Prog. Phys.* **86** (2023) 066001.
- [11] X. Yin, Partition functions of three-dimensional pure gravity, *Commun. Num. Theor. Phys.* **2** (2008) 285.
- [12] X. Yin, On non-handlebody instantons in 3D gravity, *JHEP* **09** (2008) 120.
- [13] H. Maxfield, S. F. Ross and B. Way, Holographic partition functions and phases for higher genus Riemann surfaces, *Class. Quantum Grav.* **33** (2016) 125018.
- [14] J. M. Maldacena and L. Maoz, Wormholes in AdS, *JHEP* **02** (2004) 053.
- [15] P. Betzios, E. Kiritsis and O. Papadoulaki, Euclidean wormholes and holography, *JHEP* **06** (2019) 042.
- [16] P. Betzios, E. Kiritsis and O. Papadoulaki, Interacting systems and wormholes, *JHEP* **02** (2022) 126.
- [17] M. V. Raamsdonk, Comments on wormholes, ensembles, and cosmology, *JHEP* **12** (2021) 156.
- [18] D. Marolf and J. E. Santos, AdS Euclidean wormholes, *Class. Quantum Grav.* **38** (2021) 224002.
- [19] S. Carlip, The sum over topologies in three-dimensional Euclidean quantum gravity, *Class. Quant. Grav.* **10** (1993) 207.
- [20] K. Krasnov, Holography and Riemann surfaces, *Adv. Theor. Math. Phys.* **4** (2000) 929.
- [21] L. A. Takhtajan and L.-P. Teo, Liouville action and Weil-Petersson metric on deformation spaces, global Kleinian reciprocity and holography, *Commun. Math. Phys.* **239** (2003) 183–240.

- [22] J. Park, L. A. Takhtajan and L.-P. Teo, Potentials and Chern forms for Weil–Petersson and Takhtajan–Zograf metrics on moduli spaces. *Adv. Math.* **305** (2017) 856–894.
- [23] J. Park and L.-P. Teo, Liouville action and holography on Quasi-Fuchsian deformation spaces, *Commun. Math. Phys.* **362** (2018) 717–758.
- [24] A. Maloney and E. Witten, Quantum gravity partition functions in three dimensions, *JHEP* **02** (2010) 029.
- [25] N. Iizuka, A. Tanaka and S. Terashima, Exact path integral for 3D quantum gravity, *Phys. Rev. Lett.* **115** (2015) 161304.
- [26] S. Coleman, Why there is nothing rather than something: a theory of the cosmological constant, *Nucl. Phys. B* **310** (1988) 643.
- [27] S. Carlip, Dominant topologies in Euclidean quantum gravity, *Class. Quantum Grav.* **15** (1998) 2629.
- [28] K. Skenderis and B. C. van Rees, Holography and wormholes in 2+1 dimensions, *Commun. Math. Phys.* **301** (2011) 583–626.
- [29] A. Maloney and E. Witten, Averaging over Narain moduli space, *JHEP* **10** (2020) 187.
- [30] J. Cotler, K. Jensen and A. Maloney, Low-dimensional de Sitter quantum gravity, *JHEP* **06** (2020) 048.
- [31] S. Collier and A. Maloney, Wormholes and spectral statistics in the Narain ensemble, *JHEP* **03** (2022) 004.
- [32] H. Zolfi, Complexity and multi-boundary wormholes in $2 + 1$ dimensions, *JHEP* **04** (2023) 076.
- [33] P. Saad, S. H. Shenker and D. Stanford, JT gravity as a matrix integral, [arXiv:1903.11115](https://arxiv.org/abs/1903.11115).

- [34] H. Zolfi, Complexity and multi-boundary wormholes in $2 + 1$ dimensions, JHEP **04** (2023) 076.
- [35] S. He, Y. Z. Li and Y. F. Xie, Holographic stress tensor correlators on higher genus Riemann surfaces, arXiv:2406.04042v2.
- [36] S. He, Y. Li, Y. Z. Li and Y. D. Zhang, Holographic torus correlators of stress tensor in $\text{AdS}_3/\text{CFT}_2$, JHEP **06** (2023) 116.
- [37] S. He, Y. Li, Y. Z. Li and Y. D. Zhang, Note on holographic torus stress tensor correlators in AdS_3 gravity, arXiv:2405.01255v2.
- [38] S. He, Y. Z. Li and Y. D. Zhang, Holographic torus correlators in AdS_3 gravity coupled to scalar field, JHEP **05** (2024) 254.
- [39] J. R. Espinosaa and J.-F. Fortin, Vacuum decay actions from tunneling potentials for general spacetime dimension, JCAP **02** (2023) 023.
- [40] S. R. Coleman and F. De Luccia, Gravitational effects on and of vacuum decay, Phys. Rev. D **21** (1980) 3305.
- [41] H. Wang and J. Wang, Quantum master equation for the vacuum decay dynamics, JHEP **09** (2023) 113.
- [42] M. Nakahara, Geometry, topology and physics, CRC press, Boca Raton, US (2003).
- [43] S. Giombi, A. Maloney and X. Yin, One-loop partition functions of 3D gravity, JHEP **08** (2008) 007.
- [44] C. Kiefer, Quantum gravity, Oxford University Press, Oxford, U.K. (2007).
- [45] H. Wang and J. Wang, Quantum cosmology of the flat universe via closed real-time path integral, Eur. Phys. J. C **82** (2022) 1172.
- [46] H. Wang and J. Wang, Quantum geometrical current and coherence of the open gravitation system: loop quantum gravity coupled with a thermal scalar field, Phys. Scr. **98** (2023) 045303.

- [47] L. Takhtajan and P. Zograf, On uniformization of Riemann surfaces and the Weyl-Peterson metric on Teichmüller and Schottky spaces, *Math. USSR Sbornik* **60** (1988) 297-313.
- [48] T. Hertog and G. T. Horowitz, Towards a big crunch dual, *JHEP* **07** (2004) 073.
- [49] J. L. F. Barbon and E. Rabinovici, Holography of AdS vacuum bubbles, *JHEP* **04** (2010) 123.
- [50] D. Harlow and L. Susskind, Crunches, Hats, and a Conjecture, [arXiv:1012.5302](https://arxiv.org/abs/1012.5302).
- [51] J. Maldacena, Vacuum decay into Anti de Sitter space, [arXiv:1012.0274](https://arxiv.org/abs/1012.0274).
- [52] B. Körs and M. G. Schmidt, Two loop Feynman diagrams in Yang-Mills theory from bosonic string amplitudes, [arXiv:hep-th/0003171](https://arxiv.org/abs/hep-th/0003171).
- [53] A. Lyons and S. W. Hawking, Wormholes in string theory, *Phys. Rev. D* **44** (1991) 3802.
- [54] V. A. Rubakov and D. S. Gorbunov, Introduction to the theory of the early universe, World Scientific, Singapore (2017).
- [55] S. Coleman and K. Lee, Escape from the menace of the giant wormholes, *Phys. Lett. B* **221** (1989) 242.
- [56] M. Schlichenmaier, An Introduction to Riemann Surfaces, Algebraic Curves and Moduli Spaces, Berlin: Springer-Verlag (1989).
- [57] H. Maaß, Siegel's Modular Forms and Dirichlet Series, Springer, Heidelberg Germany (1971).
- [58] N. Lu, A simple presentation of the Siegel modular groups, *Lin. Algebra Appl.* **166** (1992) 185.
- [59] X. G. Liu and G. J. Ding, Neutrino masses and mixing from double covering of finite modular groups, *JHEP* **08** (2019) 134.

- [60] F. Diamond and J. M. Shurman, A first course in modular forms, Grad. Texts Math. **228**, Springer, New York, NY, U.S.A. (2005).
- [61] G. J. Ding, S. F. King and X. G. Liu, Modular A_4 symmetry models of neutrinos and charged leptons, JHEP **09** (2019) 074.
- [62] F. Mandl and G. Shaw, Quantum field theory, Wiley, New York (1988).
- [63] J. Manschot, AdS_3 partition functions reconstructed, JHEP **10** (2007) 103.
- [64] N. Koblitz, Introduction to Elliptic Curves and Modular Forms, Springer-Verlag, Heidelberg Germany (1984).
- [65] S. P. De Alwis, F. Muia, V. Pasquarella and F. Quevedo, Quantum transitions between Minkowski and de Sitter spacetimes, Fortschr. Phys. **68** (2020) 2000069.
- [66] E. J. Weinberg, “Classical solutions in quantum field theory : Solitons and Instantons in High Energy Physics,” Cambridge Monographs on Mathematical Physics, September (2012).
- [67] H. Wang, Y. X. Wu, R. Li and J. Wang, Wormhole influence on the false vacuum bubble tunneling, arXiv:2310.00284v1.
- [68] L. M. Navas, F. J. Ruiz and J. L. Varona, Asymptotic behavior of the Lerch transcendent function, J. Approx. Theory **170** (2013) 21–31,
- [69] P. D. Vecchia, F. Pezzella, M. Frau, K. Hornfeck, A. Lerda and A. Sciuto, N point g loop vertex for a free Bosonic theory with vacuum charge Q, Nucl. Phys. B **322** (1989) 317.
- [70] L. Ford, Automorphic functions, Chelsea (1951).
- [71] S. Playle, Deforming super Riemann surfaces with gravitinos and super Schottky groups, JHEP **12** (2016) 035.
- [72] E. D. Belokolos, A. I. Bobenko, V. Z. Enolski, A. R. Its and V. B. Matveev, Algebro-geometric approach to nonlinear integrable equations, Springer, New York (1994).

- [73] L. Magnea, S. Playle, R. Russo and S. Sciuto, Two-loop Yang-Mills diagrams from superstring amplitudes, JHEP **06** (2015) 146.
- [74] S. K. Blau, E. I. Guendelman and A. H. Guth, Dynamics of false-vacuum bubbles, Phys. Rev. D **35** (1987) 1747.